

Insulator Based Dielectrophoretic Trapping of Single Mammalian Cells

by

Sanchari Bhattacharya

A Dissertation Presented in Partial Fulfillment  
of the Requirements for the Degree  
Doctor of Philosophy

Approved November 2013 by the  
Graduate Supervisory Committee:

Alexandra Ros, Chair  
Daniel Buttry  
Robert Ros

ARIZONA STATE UNIVERSITY

December 2013

## ABSTRACT

This work demonstrated a novel microfluidic device based on direct current (DC) insulator based dielectrophoresis (iDEP) for trapping individual mammalian cells in a microfluidic device. The novel device is also applicable for selective trapping of weakly metastatic mammalian breast cancer cells (MCF-7) from mixtures with mammalian Peripheral Blood Mononuclear Cells (PBMC) and highly metastatic mammalian breast cancer cells, MDA-MB-231. The advantage of this approach is the ease of integration of iDEP structures in microfluidic channels using soft lithography, the use of DC electric fields, the addressability of the single cell traps for downstream analysis and the straightforward multiplexing for single cell trapping. These microfluidic devices are targeted for capturing of single cells based on their DEP behavior. The numerical simulations point out the trapping regions in which single cell DEP trapping occurs. This work also demonstrates the cell conductivity values of different cell types, calculated using the single-shell model. Low conductivity buffers are used for trapping experiments. These low conductivity buffers help reduce the Joule heating. Viability of the cells in the buffer system was studied in detail with a population size of approximately 100 cells for each study. The work also demonstrates the development of the parallelized single cell trap device with optimized traps. This device is also capable of being coupled detection of target protein using MALDI-MS.

## DEDICATION

[Dedicated to my parents]

## TABLE OF CONTENTS

	Page
LIST OF TABLES.....	vi
LIST OF FIGURES.....	vii
CHAPTER	
<b>1. INTRODUCTION.....</b>	<b>1</b>
Dissertation Objectives.....	4
<b>2. DIELECTROPHORESIS AND GOVERNING</b>	
<b>ELECTROKINETIC EFFECTS.....</b>	<b>10</b>
Dielectrophoresis of Spherical Particles.....	10
Dielectrophoresis of Cells.....	16
<b>3. MATERIALS AND METHOD.....</b>	<b>18</b>
Chemicals.....	18
Cell Types and Culture.....	18
Cell Viability Tes.....	21
Chip Fabrication.....	21
Photolithography.....	21
Softlithography.....	22
Trapping Experiments.....	24
<b>4. THEORETICAL MODELING.....</b>	<b>25</b>

CHAPTER	Page
Generation-1.....	26
Generation-2.....	27
5. EXPERIMENTAL RESULTS AND DISCUSSION.....	32
iDEP Trap for Single Particles.....	33
Simulations.....	33
Experiments.....	35
iDEP Trap for Single Cancer Cells.....	38
Single Cancer Cell Trapping (MCF-7) in HEPES/Glycerol Buffer.....	38
Single Cancer Cell Trapping (MCF-7) in HEPES/Trehalose Buffer.....	42
Single Cancer Cell Trapping (MDA-MB-231) in HEPES/Trehalose Buffer.....	45
Experiments.....	45
Simulations.....	47
Viability Studies.....	49
Single Cancer Cell Trapping of Peripheral Blood Mononuclear Cells in HEPES/Glycerol Buffer.....	50
Selective Trapping of MCF-7 and Peripheral Blood Mononuclear Cell.....	51
Experiments.....	52
Simulations.....	53
Selective Trapping of MCF-7 and MDA-MB 231.....	57

CHAPTER	Page
Experiments.....	57
Simulations.....	58
Importance of Differential Trapping of MCF-7 and MDA-MB-231.....	60
6. CONCLUSIONS.....	61
7. APPENDIX A.....	71

## LIST OF TABLES

Table	Page
1. Geometries of trapping intersection and insulating posts of new device	
A) Generation- 2a to 2c.....	38
B) Generation-2d to 2f.....	39
2. Conductivity of phosphate buffer and $f_{CM}$ (Claussius- Mossoti factor) of polystyrene beads.....	47
3. Comparison of $f_{CM}$ , $\mu_{DEP}$ (dielectrophoretic mobility), $\sigma_p$ (cell conductivity) and $\sigma_{mem}$ (cell membrane conductivity) for the different types of cells in PBMC and MCF-7 .....	65
4. Comparison of $f_{CM}$ , $\mu_{DEP}$ (dielectrophoretic mobility), $\sigma_p$ (Cell conductivity) and $\sigma_{mem}$ (cell membrane conductivity) for the different types of cells in PBMC and MCF-7 .....	69

## LIST OF FIGURES

Figure		Page
1.	Effect of electric field on charged and neutral particle.....	7
2.	A) Schematic of electrical double layer.	
	B) Electroosmotic flow Profile in PDMS microchannel.....	9
3.	A) Polarizable particle expressing p-DEP in non-uniform electric field	
	B) Polarizable particle expressing n-DEP in non-uniform electric field.....	10
4.	A) Cross section of microchannel with metal deposition.	
	B) Simulations of electric field square value along the cross section.....	12
5.	A) Top view of microfluidic channel with cylindrical insulating posts	
	B) Horizontal cross section showing electric field lines curving around posts.	
	C) Simulation showing electric field gradient square distribution around insulating posts.....	12
6.	Single- shell model for cell to determine cell conductivity.....	17
7.	Photolithography Process, A) Spin coating SU-8.	
	B) UV exposure through Chrome mask.	
	C) Development of non-exposed SU-8.....	22
8.	Softlithography Process. A) PDMS coated master wafer.	
	B) Reservoir holes punched at the edge of straight channel.	
	C) Assembled chip after plasma treatment of glass and PDMS.....	23
9.	A) Schematic of cell trapping position in microfluidic device,	

Figure	Page
B) Cross section of iDEP trapping device .....	24
10. Simulations of tear-drop device with trapping.....	26
11. Parameters considered for developing the optimized single cell trap.....	29
12. Distribution of electric field gradient square distribution along tips of tear-drop posts of different geometries. Geometry analysis of new mask design.....	31
13. Numerical simulations of electric field gradient square distribution in device with ellipsoid insulating post.....	35
14. Snapshots of video sequence showing trapping of single bead. A) Single bead travels toward post, B) Trapped single bead.....	37
15. Plot of trapping electric field for single beads versus conductivity of the buffer.....	38
16. Numerical simulations of electric field gradient square distribution in device with tear-drop insulating posts.....	40
17. Effects of electric field on viability of MCF-7 cancer cells in HEPES/glycerol buffer. A) Comparison of live/dead cell population with electric field application. B) Normalized distribution of viable MCF-7 cells with electric field application.....	41
18. Snapshots of video sequence of single MCF-7 cancer cell trapping in HEPES/glycerol buffer. A) Cell travels toward trapping position. B) Cell gets directed toward trapping position) Single MCF-7 cell is trapped.....	43
19. Snapshots of video sequence of single MCF-7 cancer cell trapping in HEPES/trehalose buffer. A) Cell travels toward trapping position. B) Cell gets directed toward trapping position. C) Single MCF-7 cell is trapped.....	44
20. Viability of MCF-7 cells in HEPES/trehalose buffer. A) Live/dead cell population	

Figure	Page
distribution in buffer incubation. B) Live/dead cell population distribution with 100V/cm electric field application.....	45
21. Snapshots of video sequence of single MDA-MB-231 cancer cell trapping in HEPES/trehalose buffer. A) Cell travels toward trapping position. B) Cell gets directed toward trapping position. C) Single MDA-MB-231 cell is trapped.....	47
22. Simulations of trapping condition in tear-drop device for MDA-MB-231 cancer cells. A) Simulation of compete geometry. B) Simulation of are around insulating posts.....	49
23. Viability of MDA-MB-231 cells in HEPES/trehalose buffer. A) Live/dead cell populationdistribution in buffer incubation. B) Live/dead cell population distribution with 200V/cm electric field application.....	50
24. Viability of PBMC in HEPES/trehalose buffer incubation.....	52
25. Snap shot of selective trapping of MCF-7 and PBMC. A) Trapped MCF-7cell with PBMC arriving at iDEP trap. B) PBMC flow through the trap. C) PBMC flow downstream.....	54
26. Simulation of trapping region for MCF-7 and B-lymphocytes	

Figure	Page
A) Schematic of iDEP trap.	
B) Trapping condition for MCF-7	
C) Trapping condition for B-lymphocytes.....	55
 27. Viability comparison of MCF-7 and PBMC population with application of 100V/cm electric field. A) Live/dead cell population distribution of MCF-7 cells. B) Live/dead cell population distribution of PBMC -7 cells.....	56
 28. Simulation of trapping condition and snapshot sequence videos depicting selective trapping for MCF-7 and MDA-MB-231 cells. A) Trapping condition for MCF-7. B) Snapshot of trapped MCF-7. C) Trapping condition for MDA-MB-231. D)-E) Snapshot Sequence of MDA-MB-231 flow through the trapping region.....	58
 29. Simulations of trapping condition of MCF-7 and MDA-MB-231	
A) Schematic of complete intersection.	
B) Trapping condition for MCF-7 around the posts.	
C) Trapping condition of MDA-MB-231 around the posts.....	59
 30. Viability comparison of MCF-7 and MDA-MB-231 at 100V/cm	
A) Live/dead cell population distribution of MCF-7 cells.	
B) Live/dead cell population distribution of MDA-MB-231 cells.....	61

## CHAPTER 1

### INTRODUCTION

Conventional biological studies are usually carried out with large cell populations, thus preventing assessment of cell cycle dependent states or inhomogeneous responses to external stimuli. However, accessing the information inherent to single cells will allow us to resolve such heterogeneity and eventually improve the understanding of enduring problems in molecular biology, cancer diagnostics, pathology and therapy. Essential for integrated single cell analysis is the manipulation, navigation, stimulation, lysis and analysis of individual cells. Microfluidic platforms have become an important tool for single cell analysis [1-5], as they allow constructing fluidic channels in dimensions adopted to pico and femtoliter volumes and thus manipulate the volume of single mammalian cells with minimal dilution errors. Single cell traps should however, not only allow spatial localization of single cells, but also create micro-reaction chambers, where reactions with stimuli can take place and subsequent lysis can be performed. Hence, microfluidic single cell traps should be individually addressable via inlet and outlet channels and be able to transport single cell lysate to downstream separation and analysis. Ideally, single cell traps should also have the potential to be parallelized to improve statistical significance of single cell analysis.

Positioning of particles and cells in aqueous solutions has been a subject of intense investigation [6]. Various forms of manipulations have been studied for particle and cell trapping based on optical [7], magnetic [8-10], electric [11-13], hydrodynamic [14] and ultrasound [15, 16], as well as approaches based on adhesion differences [17].

Single cell manipulation devices have been demonstrated as summarized elsewhere [4, 5, 18-21]. Dielectrophoresis (DEP) is an electrokinetic technique which is capable of manipulating a wide variety of particles and cells [22, 23]. It has also become a versatile tool for trapping single cells. A variety of efficient designs have been realized in the past. Earlier studies focused on modeling single particle traps [12] and the application of single particle trapping with microspheres [24]. 3D arranged electrode designs have been proven to be versatile for trapping individual cells [25] and for contact-less cultivation of single cells using DEP [26]. More recently, effective DEP cages were realized with circular ring electrodes [27] to trap single cells. Trapping of an osteoblast-like cell has been demonstrated with similar techniques [28]. Other applications include the development of massively parallel single cell traps [29] and saw tooth electrode designs to capture single cells in a microfluidic channel [30]. Moreover, DEP has been used in combination with electrothermal effects [31], hydrodynamic forces [32] or cultivation in microwells [33]. Metal-coated micrometer sized glass tips could also be employed as dielectrophoretic tweezers to capture single cells [34].

Several studies have demonstrated the use of DEP to selectively manipulate analytically and clinically relevant cell types such as bacteria or cancer cells. Traditionally, DEP has been employed using microelectrodes and alternating current (AC) electric fields for studying DEP trapping behavior, demonstrating differences in DEP response of cell types such as dead versus live cells [35-38]. While single cell manipulation devices have been well demonstrated, the creation of a device capable of distinguishing a variety of different cell types combined with subsequent molecular

studies on the single cell level is still a major challenge. A prominent example for required selectivity with rare cells is the investigation of circulatory tumor cells in blood, which are of diagnostic relevance but are vastly outnumbered by normal cells [39-41]. Analytical applications of cell DEP thus include, but are not limited to, DEP-field-flow-fractionation (DEP-FFF) for a variety of cells [42, 43] or dielectrophoretically activated cell sorting (DACS) [44-47]. Kim *et al.* [48] have used DACS for separation of mouse embryonic carcinoma (P19EC) cells from red blood cells. They have also demonstrated separation of human MDA-435 breast cancer cells from T-lymphocytes by DEP-FFF using a rectangular chamber with microfabricated interdigitated electrodes [43].

Application of DEP for mammalian cell sorting was mainly realized in miniaturized electrode designs; however, electrode fouling imposes a limitation on the lifetime of the devices. Cummings and Singh [49] introduced the insulator-based dielectrophoresis (iDEP) technique where insulating posts are used to generate a non-uniform electric fields within microfluidic channels. This is a relatively new technique and mainly focused on particle [50-52] and microbe manipulation such as bacteria [37, 53], yeast cells [54] or spores and viruses [51]. Chen *et al.* [38] have demonstrated selective trapping of live mammalian HeLa cells in an open-top iDEP device using an AC field. Further, Kang *et al.* [55] have demonstrated separation of different sized white blood cells from human breast cancer cells (MCF-7) using DC iDEP. Lapizco-Encinas *et al.* [56] have recently demonstrated the differential DEP behavior between yeast and bacteria exploiting their cellular structure differences. A variation of iDEP was

demonstrated by Jones *et al.* [57] with a DC iDEP device consisting of saw tooth shaped insulators along the walls of a microfluidic channel to capture red blood cells.

A recent development in the field of dielectrophoresis is contactless dielectrophoresis (cDEP). In this technique, electrodes are isolated from the main fluidic channel by a thin membrane and capacitive coupling is used to provide the necessary electric field gradients. Shafiee *et al.* [58] used this technique to separate dead and live THP-1 human leukemia monocytes as well as isolate MDA-MB-231 from MCF-7 and MCF-10A by altering the frequency of an AC field [59]. More recently, the same group used this technique to determine the membrane capacitance of blood cells, macrophages, breast cancer cells and leukemia cells [58, 60].

The detection and quantification of proteins in individual cells in high throughput is of enormous biological and clinical significance. Current methods require the measurement of a large cell population or are limited to the investigation of few cells at a time. Yang *et al.* [61] demonstrated the combination of a PDMS-based microfluidic device with matrix-assisted laser desorption ionization time-of-flight mass spectrometry (MALDI-TOF-MS) that could detect 300 molecules at the peptide level and  $\sim 10^6 - 10^7$  molecules at the protein level. This reported detection limit is close to the requirements of analyzing protein and peptides originating from few or even single cells.

## 1.1 Dissertation objective

The purpose of this dissertation is to demonstrate the development and significance of a novel microfluidic device which is a combined platform for trapping single cancer cells utilizing DC iDEP, followed by downstream MALDI MS analysis of target proteins. The complete platform for the novel device is given in Figure 1.

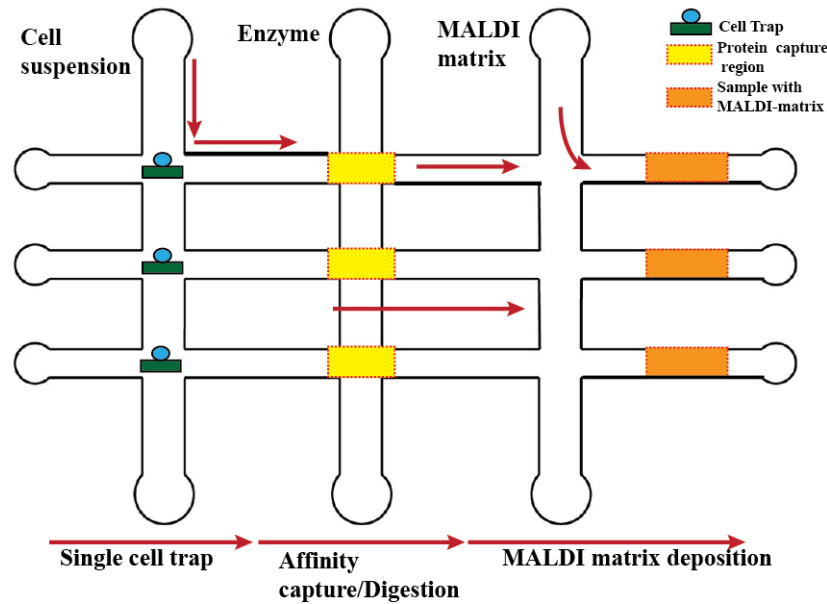


Figure 1: Complete microfluidic platform for single cell trapping and target analyte analysis. Single cells are trapped at desired locations followed by manipulation with lysing agents. Affinity capture region captures the target protein followed by mixing with MALDI-MS matrix for analysis.

As shown in Figure 1, the device is the complete microfluidic platform for trapping a single cell and analyzing target proteins. This thesis is based on the trapping of a single cancer cell at a desired location followed by manipulation of the cell. The design of the device addresses the ease of integration of iDEP posts inside the microfluidic channels using soft lithography. The novel device consists of four channels forming an

intersection where insulating post(s) deform the electric field gradient and thus invoke DEP. Several devices were designed for invoking negative DEP (n-DEP) or positive DEP (p-DEP) at the intersection of the channel by altering the post geometries. The novel device was successful in trapping a single mammalian MCF-7 cancer cell and also selective trapping of MCF-7 cells from a mixture with another type of breast cancer cell, MDA-MB-231, and peripheral blood mononuclear cells.

CHAPTER 2  
DIELECTROPHORESIS AND GOVERNING  
ELECTROKINETIC EFFECTS

Several forces act upon a polarizable particle suspended in a conductive medium with the application of an electric field. The electrophoretic velocity is due to the charge of the particle and is negligible for uncharged particles. The dielectrophoretic force on the particle is due to the polarization effects on the particle and the medium. These forces govern the resultant velocity of the particle with respect to the medium in the microfluidic channel. Other contributing factors are Brownian motion and pressure gradient flow in the channel due to uneven fluid volumes in the reservoirs. The latter can be reduced by using equal volumes of fluid in the reservoir. For particles with a large radius like cells, Brownian motion can be neglected with respect to the other forces for simplification.

Electrophoresis is a common electrokinetic separation technique [62]. It is a phenomenon where the charged particles move along the electric field lines. For example in Figure 2, the negatively charged particle (A) moves toward the positive electrode whereas the neutral particle (B) remains stationary because the force acting on the particles from both positive and negative electrodes are equal in magnitude and opposite in direction.

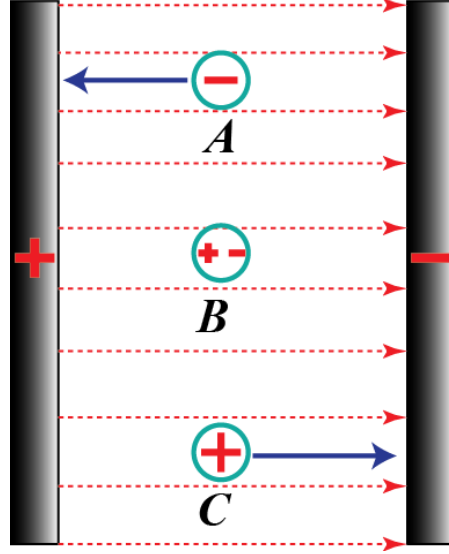


Figure 2: Effect of a uniform electric field on charged particles *A* and *C* and a neutral particle *B* depicting movement of the charged particles along electric field lines while the neutral particle remains stationary.

The electrophoretic mobility on a particle of radius  $r$  is as follows:

$$\mu_{DEP} = \frac{q}{6\pi\eta r} \quad (1)$$

where  $\eta$  is medium viscosity and  $q$  is particle charge. The separation techniques exploit the difference in charge  $q$  and size  $r$  of particles for differential migration of particles through a medium. The electrophoretic velocity of the particle  $v_{EP}$  in electric field  $\mathbf{E}$  is as follows:

$$\mathbf{v}_{EP} = \mu_{EP}\mathbf{E} \quad (2)$$

It is important to consider the electrical double layers on the surface of the particle which alters the effective net charge on the particle [63] along with that of the channel wall. Electrophoretic separation experiments starts with localized injection of a sample at

the start of the separating medium. When an electric field is applied, analytes having different electrophoretic mobilities migrate with different velocities (Eq. 2) and separate in space. Spatial detection of the separated species is performed with imaging techniques (whole column scans or staining techniques) or temporal detection by fixed point detectors (absorbance, fluorescence, etc.) where migrating species pass at different times [64, 65].

In addition to electrophoresis, the walls of systems with small cross sections produce electroosmotic flow (EOF). Polydimethylsiloxane (PDMS) substrate is used for making microfluidic devices described in this work. Prior to assembly, the PDMS is plasma treated and then covalently bonded to a plasma-treated glass surface to form a well-sealed microfluidic channel. Plasma treatment of the PDMS generates negative charges on the surface. This is due to the de-protonation of the silanol groups of the PDMS walls. [66].

These negative charges on the PDMS surface attract the counterions from the buffer. The ions directly attached to the surface of the PDMS wall and form an immobile layer called the Stern layer. The mobile layer is called the diffusive layer and contains ions of both charges but enriched in one, depending on the surface charge. The two layers combined form the electric double layer or Debye layer ( $\lambda_D$ ). Figure 3A shows the Stern model of the electrical double layer. When an external electric field ( $E$ ) is applied to a microchannel filled with a buffer the charge on the Debye layer gets accelerated across the channel as shown in Figure 3B. These ions migrate towards the cathode, moving the bulk solution by viscous drag.

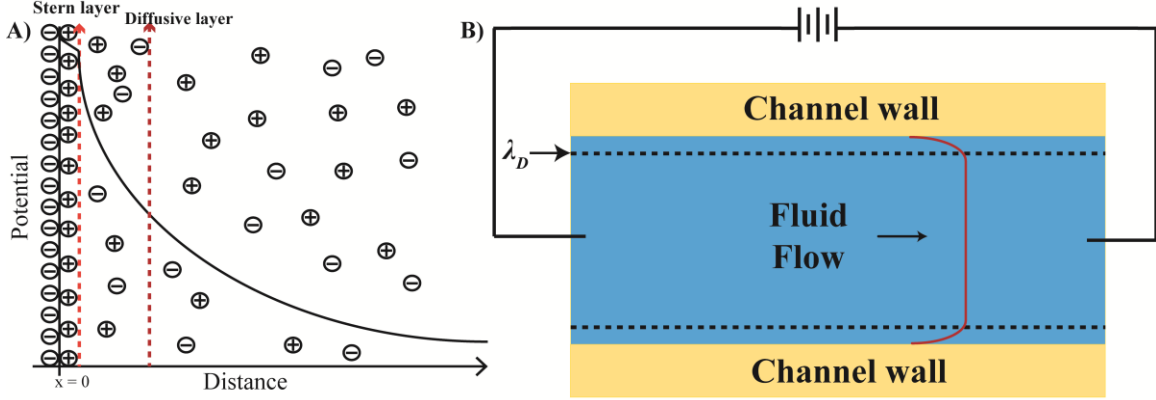


Figure 3: (A) The immobile layer formed at the immediate vicinity of the PDMS wall is the Stern layer. The other layer is mobile and denoted the Diffusive layer. The electrostatic potential decreases linearly through the stern layer and then exponentially (as indicated by the black line). (B) Scheme showing the electroosmotic velocity profile of the fluid. Upon application of an electric field, a bulk flow arises exhibiting a flat velocity profile.

The shear force in the liquid leads to the electroosmotic bulk flow in the channel.

The electroosmotic velocity  $\mathbf{v}_{EOF}$ , is given by the Smoluchwsky equation:

$$\mathbf{v}_{EOF} = \frac{\mathbf{E} \varepsilon_{med} \xi}{\eta} \quad (3)$$

where  $\xi$  is the zeta potential,  $\varepsilon_{med}$  is medium permittivity, and  $\eta$  is the medium viscosity.

In a microfluidic channel of length  $L$ , the  $\mathbf{v}_{EOF}$  is given as:

$$\mathbf{v}_{EOF} = \frac{L}{t} \quad (4)$$

where  $t$  is the time required for the fluid to travel a distance  $L$ . The EOF mobility ( $\mu_{EOF}$ )

is given as:

$$\mu_{EOF} = \frac{v_{EOF}}{E} \quad (5)$$

The electric field  $E$ , is given as:

$$E = \frac{V}{L} \quad (6)$$

where  $V$  is the potential applied. Combining Eq. 5 and 6, the  $\mu_{EOF}$  is given as:

$$\mu_{EOF} = \frac{L^2}{Vt} \quad (7)$$

This equation is used to determine EOF in the device using well defined parameters and applied potentials.

## 2.2 Dielectrophoresis of spherical particles

The term “Dielectrophoresis” was coined by H. A. Pohl [67]. It is derived from the Greek word for force meaning “Phoresis” and “Dielectric” which is polarizable material. Pohl derived it from the term “electrophoresis” which is used to describe the motion of electrically charged particles. Dielectrophoresis (DEP) is the translational motion of polarizable particles caused by polarization effects in a non-uniform electric field. For example in Figure 4A, the polarized particle moves toward the region of high electric field gradient, termed positive DEP (p-DEP). In Figure 4B, the particle moves toward the region of low electric field gradient, termed negative DEP (n-DEP).

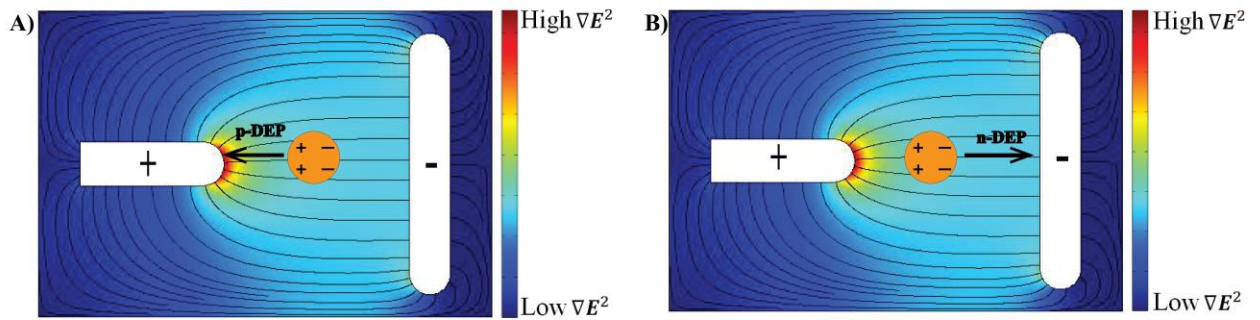


Figure 4. Effect of a non-uniform electric field on polarizable particles. Electrodes of different geometry create the non-uniform electric field. Electric field lines are shown as black lines. The color legend describes the electric field gradient squared ( $\nabla E^2$ ) distribution in the area between the electrodes. (A) A polarized particle moves toward the high electric field gradient, expressing p-DEP. (B) A polarized particle moves toward the low electric field gradient, expressing n-DEP.

Applied electric fields induce dipole movement and thereby induce an electric field along polarizable particles. The DEP force is exploited in different ways to achieve sample separation. It is an excellent approach to target the intricate parameters of the polarizability, in contrast to other electrokinetic techniques that target charge and size.

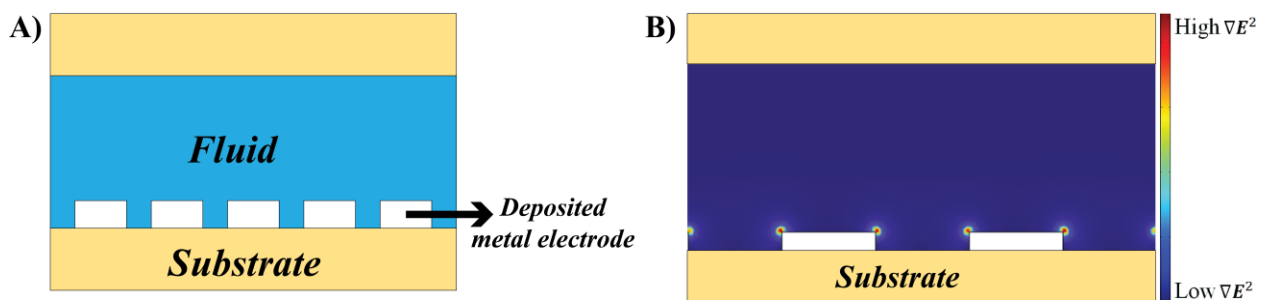


Figure 5: (A) Cross section of a microfluidic channel with metal deposited on the substrate surface. (B) Simulation of the electric field gradient squared value along the cross section of the channel. The color legend describes distribution around metallic posts.

Microelectrode-based dielectrophoresis is a widely used technique in microfluidic devices. The microelectrodes are generated by metal deposition on the substrate of the microfluidic device (Figure 5A). The electric field gradient varies along the depth of the channel (Figure 5B).

Insulator-based dielectrophoresis (iDEP) generates the non-uniform electric field due to the presence of insulators inside the fluidic channel as shown in Figure 6. The geometry of the insulating posts affects the distortion of the electric field.

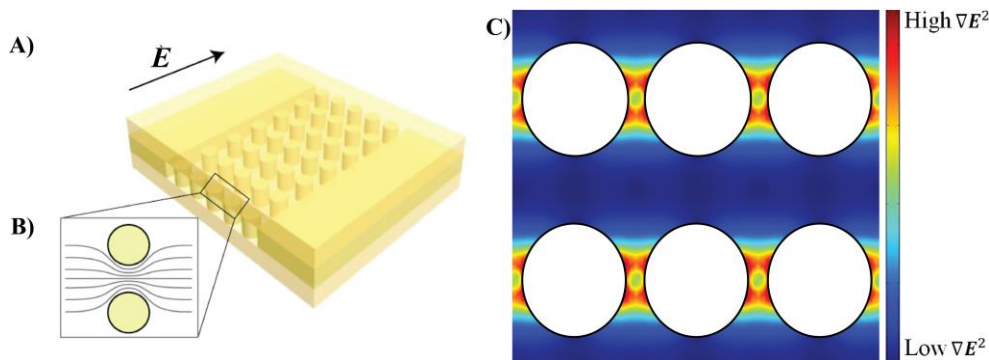


Figure 6: (A) Top view of a microfluidic channel with cylindrical insulating posts. The height of the insulating posts is the same as the channel wall. (B) Horizontal cross section of the channel showing electric field lines curving around insulating posts. (C) Simulation of the cross section of the channel depicting the  $\nabla E^2$  distribution around the insulating posts.

As evident from Figure 6A, the insulating posts are of the same height as that of the substrate wall. The electric field lines curve around the insulating posts thereby invoking the non-uniform electric field (Figure 6B). This non-uniform electric field invoked around the insulating posts remains unchanged along the depth of the

microfluidic channel. Figure 6C shows the horizontal cross section of the channel with the application of an electric field.

Dielectrophoresis is the translational motion of polarizable particles caused by polarization effects in a non-uniform electric field. The DEP force on a lossless dielectric spherical particle of radius  $r$  suspended in a medium with permittivity  $\epsilon_{med}$ , is given as [67, 68]:

$$\mathbf{F} = 2\pi\epsilon_{med}\epsilon_0r^3f_{CM}\nabla E^2 \quad (8)$$

The  $f_{CM}$  is termed the Clausius-Mossoti factor and is given as:

$$f_{CM} = \frac{\epsilon_p^* - \epsilon_{med}^*}{\epsilon_p^* + 2\epsilon_{med}^*} \quad (9)$$

where  $\epsilon_p^*$  is the complex permittivity of the particle and  $\epsilon_{med}^*$  medium permittivity. The complex permittivity of a material is given as:

$$\epsilon^* = \epsilon - \frac{i\sigma}{\omega} \quad (10)$$

Under DC conditions, the frequency dependent terms tend towards zero and  $f_{CM}$  can be expressed in terms of the conductivities of the particle and medium:

$$f_{CM} = \frac{\sigma_p - \sigma_{med}}{\sigma_p + 2\sigma_{med}} \quad (11)$$

where  $\sigma_p$  is particle conductivity and  $\sigma_{med}$  is medium conductivity. The sign of the  $f_{CM}$  indicates whether the particle will express n-DEP or p-DEP. Particles with higher

conductivity than the medium will express p-DEP and particles with lower conductivity than the medium will express n-DEP.

The DEP velocity  $\mathbf{v}_{DEP}$  for a spherical particle can be derived by balancing the frictional force on the spherical particle with the DEP force [50, 69] and is given as:

$$\mathbf{v}_{DEP} = \frac{\mathbf{F}}{f} \quad (12)$$

where  $f$  is the frictional factor of a spherical particle with radius  $r$  in a medium with viscosity  $\eta$ :

$$f = 6\pi\eta r \quad (13)$$

Substituting Eq. 8 with  $f$  from Eq. 13, one obtains:

$$\mathbf{v}_{DEP} = \mu_{DEP} \nabla E^2 \quad (14)$$

where  $\mu_{DEP}$  is the DEP mobility of the particle. The DEP mobility can thus be expressed as:

$$\mu_{DEP} = \frac{r^2 \varepsilon_{med} \varepsilon_0 f_{CM}}{3\eta} \quad (15)$$

In order to achieve immobilization of a particle due to DEP, its contribution to the particle's motion must overcome other transport mechanisms such as diffusion and electrokinetic transport (electrophoresis and electroosmosis). For the microfluidic systems considered in this work, it is assumed that the main contribution to the particles flux ( $\mathbf{J}$ ) along the microchannel arises from electrokinesis (electrophoresis and

electroosmosis), dielectrophoresis and diffusion. Diffusion of the cells is neglected due to their larger size and lower diffusion coefficients. The condition for immobilization is that the flux of the particles along the electric field is zero at the trapping regions. This is given as [50]:

$$\mathbf{J} \cdot \mathbf{E} = 0 \quad (16)$$

The flux of the particles is given by:

$$\mathbf{J} = c[\mathbf{v}_{EK} + \mathbf{v}_{EOF}] \quad (17)$$

Combining Eq. 17 and 16, one obtains:

$$c[\mathbf{v}_{EK} + \mathbf{v}_{DEP}] \cdot \mathbf{E} = 0 \quad (18)$$

where  $c$  is the concentration of the particles. Replacing the velocities with the corresponding mobilities:

$$c[\mu_{EK}\mathbf{E} - \mu_{DEP}\nabla E^2] = 0 \quad (19)$$

Rearranging Eq. 19, one obtains:

$$\left(\frac{\mu_{DEP}}{\mu_{EK}}\right) \frac{\nabla E^2}{E^2} \cdot \mathbf{E} = 1 \quad (20)$$

For DEP trapping:

$$\left(\frac{\mu_{DEP}}{\mu_{EK}}\right) \frac{\nabla E^2}{E^2} \cdot \mathbf{E} \geq 1 \quad (21)$$

Eq. 21 is used for the determination of the DEP trapping condition of particles and cells in the microfluidic channels.

### **2.2 1. Dielectrophoresis of Cells**

The cell is a complex entity with a conductive membrane and highly conductive cytosol. Models used to predict the conductivity of polystyrene spheres cannot be applicable to cells. Also, models that consider the cell as one conductive entity (Protoplast model) cannot be applicable as there is a substantial difference between the cell membrane and the cytosol conductivities. It is therefore important to determine the conductivities of the cell for understanding the trapping behavior in the device. Determination of the cell conductivity is also important for the explanation of the differential trapping behavior between cell types. MCF-7 and MDA-MB-231 cancer cells have similar size and shape and are both mammalian breast cancer cells with metastatic tendencies. The differential trapping of these two types of cancer cells is due to differences in their cell conductivities (Table 2) predicted by the single shell model.

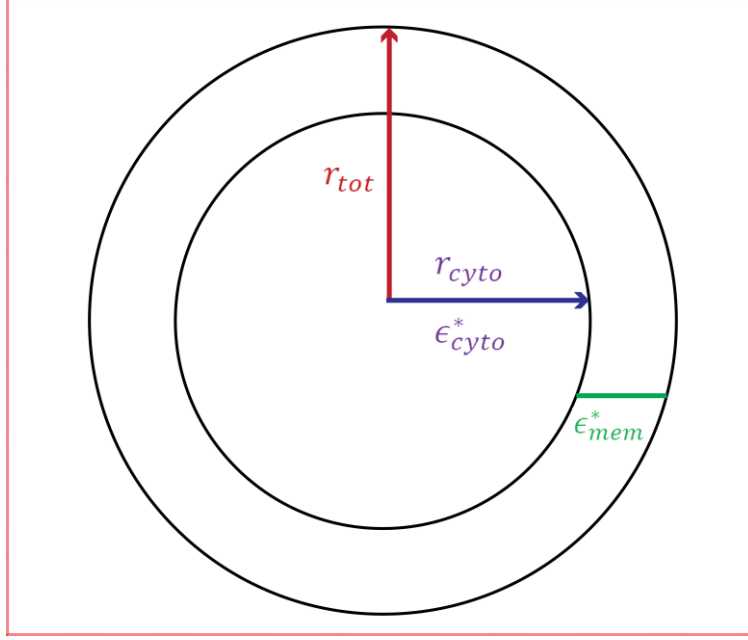


Figure 7: The concentric outer shell and inner core have permittivities  $\epsilon_{mem}^*$  and  $\epsilon_{cyto}^*$ , respectively. The particle radius is  $r_{tot}$  and the core radius is  $r_{cyto}$ .

This model can be used to determine the cell conductivity by considering the cell to be composed of two concentric layers [68]: the cytosol as a dielectric sphere covered with a cell membrane of uniform thickness, as shown in Figure 7.

The dielectric permittivity value of  $\epsilon_{p,single-shell}^*$ , replaces  $\epsilon_p^*$  in the Clausius-Mossotti factor Eq. 9[68].

$$\epsilon_{p,single-shell}^* = \epsilon_{mem}^* \frac{\left(\frac{r_{tot}}{r_{cyto}}\right)^3 + 2 \left(\frac{\epsilon_{cyto}^* - \epsilon_{mem}^*}{\epsilon_{cyto}^* + 2\epsilon_{mem}^*}\right)}{\left(\frac{r_{tot}}{r_{cyto}}\right)^3 - \left(\frac{\epsilon_{cyto}^* - \epsilon_{mem}^*}{\epsilon_{cyto}^* + 2\epsilon_{mem}^*}\right)} \quad (22)$$

For DC conditions, the corresponding permittivities are replaced by the conductivities of the cell. The cell conductivity ( $\sigma_{p,single-shell}$ ) is thereby given as:

$$\sigma_{p, \text{single-shell}} = \sigma_{mem} \frac{\left(\frac{r_{tot}}{r_{cyto}}\right)^3 + 2 \left(\frac{\sigma_{cyto} - \sigma_{mem}}{\sigma_{cyto} + 2\sigma_{mem}}\right)}{\left(\frac{r_{tot}}{r_{cyto}}\right)^3 - \left(\frac{\sigma_{cyto} - \sigma_{mem}}{\sigma_{cyto} + 2\sigma_{mem}}\right)} \quad (23)$$

The Clausius-Mossotti factor becomes:

$$f_{CM} = \frac{\sigma_{p, \text{single-shell}} - 2\sigma_{med}}{\sigma_{p, \text{single-shell}} + 2\sigma_{med}} \quad (24)$$

This model is used for predicting the total cell conductivity in this work.

## CHAPTER 3

### MATERIALS AND METHODS

#### 3.1 Chemicals

Sodium phosphate dibasic, potassium phosphate mono- basic, acetone, glycerol and isopropyl alcohol were from Sigma-Aldrich, USA, as well as 4-(2-hydroxyethyl)-1-piperazineethanesulfonic acid (HEPES) and poly(ethylene glycol)- block-poly(propylene glycol)-block-poly(ethylene glycol) with brand name Pluronic F108. Polystyrene beads of 10  $\mu\text{m}$  diameter (1% w/v in aqueous suspension) were purchased from Spherotech, USA. Tridecafluoro-1,1,2,2-tetrahydrooctyl trichlorosilane (TDTS) was from Gelest, USA. Poly(dimethyl- siloxane) (PDMS, Sylgard 184) was obtained from Dow Corning, USA and glass microscopy slides were purchased from Fisher Scientific, USA. SU-8 developer solution and SU-8 photoresist were obtained from Microchem, USA. D-(+)-Trehalose dihydrate was purchased from MP Biomedical, USA. Tridecafluoro-1,1,2,2-tetrahydrooctyl trichlorosilane (TDTS) was from Gelest, USA.

#### 3.2 Cell Types and Culture

MCF-7 breast cancer cells and PBMC were cordially provided in 1X PBS medium from the Lake-group at Arizona State University (School of Life Sciences, Tempe, USA). MDA-MB-231 breast cancer cells were cordially provided in 1X PBS

medium from the Ros group at Arizona State University (Department of Physics, Arizona State University, Tempe, USA)

MCF-7 cells (ATCC, Manassas, VA) were cultured in a solution of Eagle's Minimum Essential Medium (EMEM) (ATCC, Manassas, VA) with L-Glutamine, 10% (volume) fetal bovine serum (ATCC, Manassas, VA) and 0.01 mg/mL of bovine insulin (Sigma) and used for experiments 120 h after passaging. In addition, MDA-MB-231 cells transfected with the fluorescent protein dTomato (received from Owen McCarty, Oregon Health & Science University) were cultured in a solution of 10% (volume) fetal bovine serum (ATCC, Manassas, VA) and Dulbecco's Modified Eagle Medium (DMEM) with D-Glucose and L-Glutamine (Gibco, Invitrogen) and used for experiments 72 hours after passaging. The cells were stripped from the growth medium with a trypsin-based stripping solution and suspended in 1X PBS buffer.

The Peripheral Blood Mononuclear Cells (PBMC) samples contain mainly B-lymphocytes, T-lymphocytes and Natural Killer (NK) cells. The whole blood sample is diluted with 1X PBS (Mediatech) to twice its volume. Separating media (Ficoll, GE Healthcare) is added and mixed slowly. The blood is centrifuged at 25°C for 35 min at 1900 RPM in a Beckman Coulter Alegra (X-15R) centrifuge. Four distinct layers are formed after the centrifugation process. The second layer is aspirated out using a serological pipette. This layer is washed three times with 1X PBS at 1200 RPM at 4°C for 10 min. In the final step, the supernatant is aspirated out and the cell pellet is re-suspended in the working buffer.

### 3.2.1 Cell Viability Test

MCF-7 breast cancer cells, B-lymphocytes and MDA-MB-231 cancer cells were supplied in PBS medium. 25 ml of a PBS cell solution contained ~6 million MCF-7 cells and  $3 \times 10^7$  B-lymphocytes. 10 ml of the MDA-MB-231 PBS cell solution contained ~2 million cells. Exchange to the working buffer (30 mM HEPES/120 mM trehalose, pH = 5.1,  $\sigma_{med} = 12.5 \mu\text{S}/\text{cm}$ ) was performed by centrifugation (5 min at 1000 RPM) and replacement of supernatant with the corresponding buffer, followed by re-suspension. Ethidium homodimer-1 (EthD-1) and Calcein-AM kit (Life Technologies, USA) were used as dead/live cell stains. Cells were suspended in the working buffer of 30 mM HEPES/70 mM glycerol or 30mM HEPES/120mM trehalose containing 1mM F108 along with the cell staining solution containing 0.05% (v/v) of Calcein-AM and 0.2% (v/v) of EthD-1 (prepared according to manufacturer's protocol) and incubated for 20 min. 70  $\mu\text{L}$  of the cell suspension in the above working buffer were placed in the inlet reservoir corresponding to  $2 \times 10^4$ ,  $8 \times 10^4$  and  $1.3 \times 10^5$  MCF-7, PBMC and MDA-MB-231 cells, respectively. Cell imaging was performed at specific time intervals with potentials applied to the inlet, outlet, and side channel reservoirs corresponding to the trapping potentials at random positions. Images were captured using a dual color filter set (GFP/DsRed-A-000, Semrock, US) in a IX71 fluorescence microscope (Olympus) specific for the two cell stains (468/34 nm Ex., 512/23 nm Em. and 553/24 nm Ex., 630/91 nm Em.),. The wavelengths are separated with an Optosplit equipped with a 655/40 nm (FF01, Semrock, USA) and 510/20 nm band pass filter (FF03, Semrock, USA) and a dichroic mirror (FF580FDiO1, Semrock, USA) on two spatially different

regions of the imaging sensor adapted to the emission wavelengths of the two dyes. Approximately 100 cells within the channel and reservoir were probed to assess viability.

### 3.3 Chip Fabrication

#### 3.3.1 Photolithography

Soda lime photomasks were designed in AutoCAD (Autodesk, USA) and manufactured by Photosciences (USA). Photolithography with SU-8 photoresist was used to fabricate master wafers exhibiting the negative relief of the final microchannel design as shown in Figure 8. From those, PDMS molds were produced to obtain the final microchip.

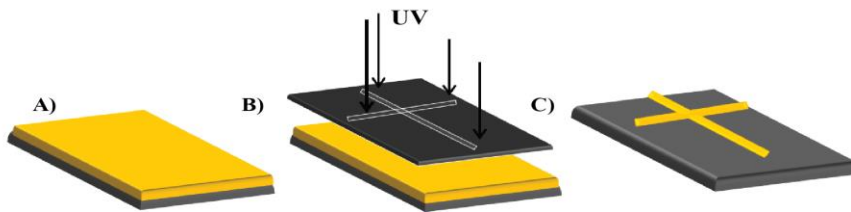


Figure 8: (A) Shows SU-8 spin coated Si-wafer substrate. (B) UV exposure of the SU-8 through a chrome mask. (C) Development of the non-exposed SU-8 using SU-8 developer, exposed relief features remain on the wafer.

The Si-wafer was spin coated with the photoresist SU-8 2005 (Microchem) at 500 RPM for 10 s and then for a further 30 s at 2000 RPM followed by a pre-exposure baking at 64°C for 1 min and 94°C for 3 mins on a hot plate (Torrey Pines, HS40A, USA). UV exposure with the photomask (Photosciences, USA) was performed on a HTG mask aligner (Hybrid Technology Group, USA) through the designed mask. The wafer was

then baked at 94°C for 5 min and subsequently developed in the SU-8 developer solution. This resulted in a patterned photoresist thickness of 35  $\mu\text{m}$ . The finalized wafer was silanized with TDTS for 30 min under vacuum in a desiccator.

### 3.3.2 Softlithography

PDMS is used for using fabrication of the chips. For PDMS molding, pre-polymer was mixed with its curing agent in a 10:1 ratio by weight, poured on the master wafer and heated at 80°C for ~ 4 h after degassing under vacuum for 30 min, shown in Figure 9.

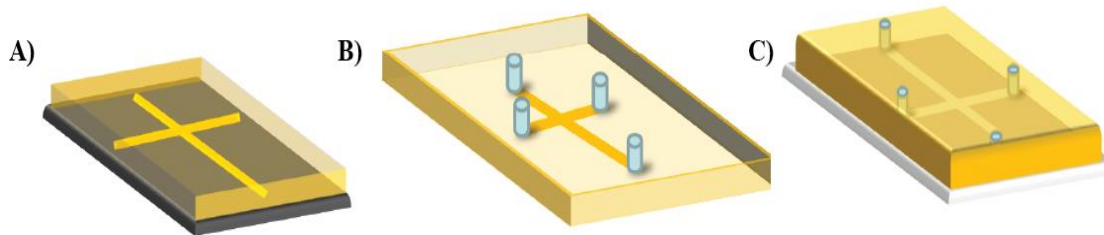


Figure 9: (A) Shows PDMS coated master wafer (B) Holes are punched at the edges of the straight channel. These holes are the fluidic reservoirs of the final chip. (C) The final chip assembled after plasma treatment of the glass and PDMS substrate to form the seal between the two surfaces. The reservoirs remain open and accessible for fluid manipulation using Pt electrodes dipped in the fluid.

The PDMS mold was then removed and holes with 2 mm diameter were punched manually at the ends of the channels to create fluid inlets. The PDMS slab and a clean glass slide (50×25 mm) were treated 30 s in an oxygen plasma oven (PDC-100 Harrick, Harrick Plasma, US) and assembled immediately after treatment. The cross-section of the complete chip is shown in Figure 10A).

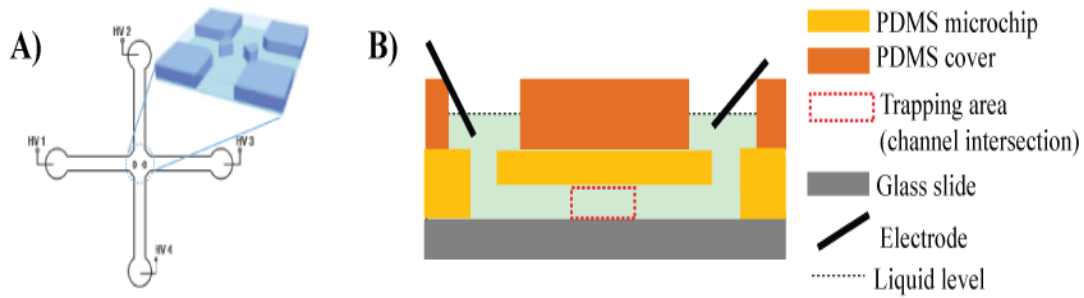


Figure 10: (A) Schematics of the cell trapping position in a microfluidic platform consisting of four channels (not to scale). The enlargement shows an example of the single cell iDEP trap and the insulating posts at the channel intersection containing teardrop posts designed for positive iDEP. Each channel can be addressed electronically via electrodes immersed in the channel reservoirs indicated as HV 1-4. (B) Cross-section of the iDEP trapping device (not to scale). The PDMS microfluidic device is sealed with a glass slide and electrodes are provided to the microfluidic reservoir with an additional PDMS holder. The liquid level (dashed line) demonstrates that electrodes are immersed in the solutions contained in the reservoir. The red rectangle represents the trapping position at the intersection of all four channels.

The assembled chip consists of a cross with four equidistant arm lengths of 0.5 cm and a channel width of 80  $\mu\text{m}$ . The insulating post(s) are located within the middle of the intersection (Figure 10A) and have a base axis length of 35 and 20  $\mu\text{m}$ . The base of the teardrop structures had a length of 25  $\mu\text{m}$  at the straight edges and a length of 28  $\mu\text{m}$  for the maximum distance from the round edge to the tip. The distance between the opposing tips of the two teardrops was 35  $\mu\text{m}$ .

An electrode holder was constructed from an additional PDMS slab of approx. 1 mm thickness holding Pt wires (0.3 mm thickness, Alfa Aesar, USA) in additionally punched reservoir holes and attached to the PDMS chip. The electrodes were connected to micro-clamps (LabSmith, USA) and voltages were applied via an HV sequencer

(HVS448 6000D, Labsmith, USA). The complete device cross-section is shown in figure 10B.

### **3.3.3 Trapping Experiments**

Assembled chips were filled by vacuum suction with corresponding buffer solutions containing Pluronic F108 at 1 mM concentration serving as a surface coating agent. The buffer concentration and conductivity were varied and conductivity was measured with a conductivity meter (Orion 3 Star, Thermo Scientific, USA). Either beads or cells were added to the inlet reservoir and a steady ramp was applied between inlet and outlet until trapping of beads or cells was observed. Video sequences of cell and bead trapping were grabbed with an inverted microscope (IX74, Olympus, USA) in brightfield with a CCD camera (Quantum 512SC, Photometrics, Tucson, AZ, USA) at a frame rate of 200 ms using Micro-Manager acquisition software (University of California, San Francisco, USA, version 1.3). A MCF-7 cell trapping experiment typically lasted 90 s. For the viability study, the electric field was applied for two periods of 2 min each and dead/live cell counts were performed after each period. Control measurements were conducted before and after the electric field application. The control measurement was conducted with a population of 100 cells at 45 min without application of an electric field. Each experiment was repeated three times with approximately 100 cells for each measurement.

## CHAPTER 4

### THEORETICAL MODELING

A single cell trap delicately balances between the electrokinetic and dielectrophoretic forces acting on the particle in the microfluidic devices. The trapping condition for any particle expressing n-DEP is given in Eq. 21, which depicts the areas within the device where single cell trapping is possible. COMSOL Multiphysics software was used to compute the DEP trapping positions of the devices.

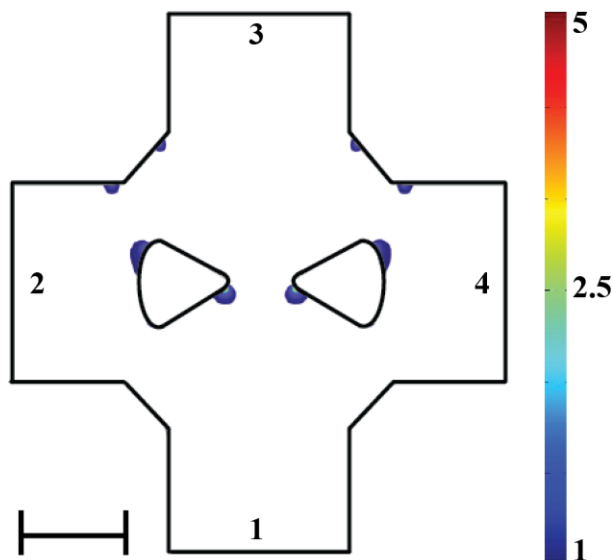


Figure 11: Simulation of tear-drop device with trapping conditions. Potentials were applied to 1, 2, 3 and 4 according to the trapping experiment. Color scale bar indicates regions where the trapping condition is greater than one. Scale bar is 50  $\mu\text{m}$ .

Figure 11 depicts the trapping regions of MDA-MB-231 cells. The applied potentials at each reservoir (boundary) of the channel were adapted to match our experimental conditions (see Results section for details). The cells express n-DEP behavior and the

trapping behavior is well explained using Eq. 21 and the simulation. This device is the first generation (Generation-1) and has been used successfully for trapping single cancer cells. A detailed explanation of the COMSOL simulation is given in Appendix 1.

## **4.2 Generation-1**

Initial designs applied for trapping experiments are termed as Generation-1 devices and have been applied to single cancer cell trapping. An ellipsoid device is designed for particles with n-DEP. AutoCAD design software is used to draw the geometries of the insulating posts because it gives better control over the geometry manipulation compared to COMSOL. The inlet, outlet and side channels are specified as conductive surfaces and the rest of the structure is specified as insulating with no-slip conditions at the wall. The inlet, outlet and side channels are open boundaries. The Reynolds number for our system is well below 1 hence the flow is considered creeping flow. The detailed description of the simulation process is given in Appendix A.

Draw backs of Generation-1:

- a) One of the draw backs for the Generation-1 devices is non-selective trapping regions near sides of the channel walls. The sharp edges of the trapping intersection generate high  $\nabla E^2$  values which create non-specific trapping at the edges of the intersection as shown in Figure 11.

- b) The final design is intended to have parallelized single cell trapping. For statistical significance of the single cell analysis, parallelized trapping of single cells is required. The first generation devices fail to address this issue.
- c) Addressing the trapping region for manipulating the trapped single cell is required for further applications. A fifth channel is required which can be used for this purpose, without disturbing the fluid flow in the rest of the channel. Although a fifth channel is present in the Generation-1 devices, it fails to give good addressability to the trapping region.

### **4.3 Generation-2**

Most of the draw backs of the Generation-1 device are addressed in the Generation-2 devices. The geometry for the entire second generation device was analyzed and the best structure was used for designing a parallelized trapping device. Insulating post geometry is critical for optimizing trapping. Several other parameters were optimized for creating the best single cells traps and preventing non-selective trapping regions seen in the Generation-1 device. The Generation-2 devices were designed with rounder outer edges  $r_0$  and a round intersection wall. Some of the characteristic features of the intersection and of the posts that were considered during the development process are given in Figure 12. The post distance is one of the important factors to be considered during development of the device. The optimized distance generated the electric field gradient required for trapping. Also, the distance of the posts from the channel wall

intersection is important. Distortion of the electric field around the posts also creates electric field gradients near the channel wall intersection. This results in undesired trapping conditions near the wall. Curving of the intersection channel walls and placing the posts at an optimized distance reduces such effects.

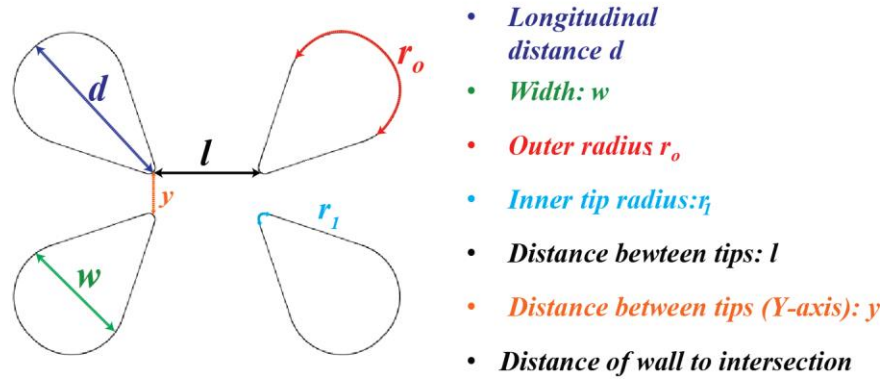
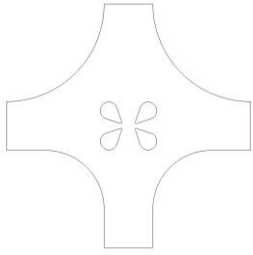
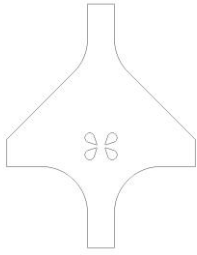
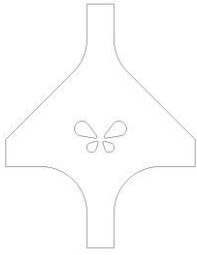


Figure 12: Parameters considered for developing the optimized single cell trap. The tear drop insulating posts are considered for the Generation-2 device. Tip geometry and post distance are the two most important factors considered.

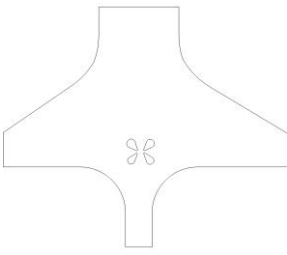
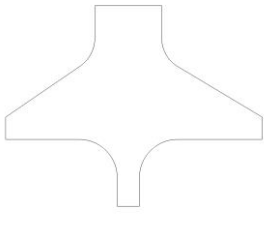
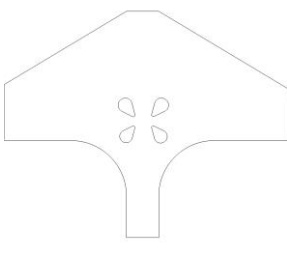
The main aspect of the geometry under consideration is the radius of the tips ( $r_1$ ) of the tear drop posts. Several geometries were tested and are shown in Tables 1A and 1B.

**Table 1A**

Generation-2a	Generation-2b	Generation-2c
		

Generation-2a to 2c are shown at the channel intersection

**Table 1B**

Generation-2d	Generation-2e	Generation-2f
		

Generation-2d to 2f are shown at the channel intersection

A cutline is drawn across the tips of the tear drop post along the length  $l$  to encompass high  $\nabla E^2$ . Figure 13 shows the plot of  $\nabla E^2$  along the tip of the posts.

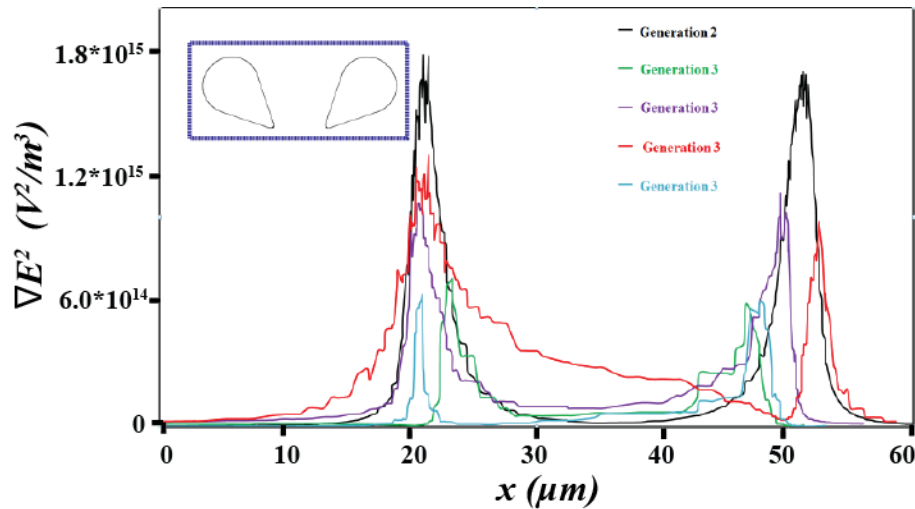


Figure 13: Distribution of  $\nabla E^2$  along the tip of the tear drop posts. The values are taken along a straight line touching the inside and areas near the tip with the highest  $\nabla E^2$  values. The outer posts were considered, as trapping regions were concentrated along the edges of these posts.

As evident from the plot in Figure 13, Generation-2a gives the highest value of  $\nabla E^2$ . This geometry was chosen for further simulation for the trapping condition (Eq. 21). The trapping condition was met at the constriction of the intersection near the outlet of the same geometry (Generation-2a) constructed in COMSOL and AutoCAD (exported to COMSOL). This was a result of an artifact of the drawing with COMSOL which was solved by constructing the geometry in AutoCAD and exporting the geometry to COMSOL.

A modification of this geometry is the application of two tear drop posts instead of four such posts. This would leave a greater exposed area under the trapped cell which would facilitate access to the cell by lysing agent and a better unobstructed passage of the

cell analyte to the side channels for further analysis. The complete geometry of the trapping device is shown in Figure 14.

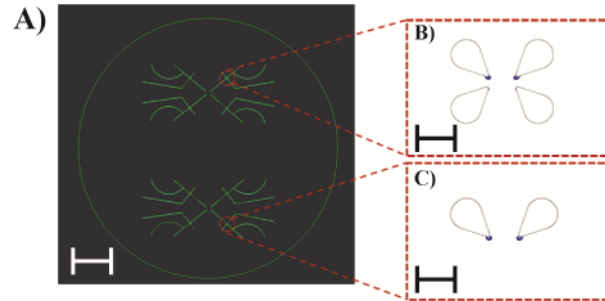


Figure 14: (A) Complete geometry of the new mask. Straight lines radially protrude out from a central inlet. Scale bar is 5  $\mu\text{m}$  (B) The trapping devices containing four tear drop insulating posts. (C) Trapping devices with two tear drop insulating posts. Scale bar is 20  $\mu\text{m}$ .

The central inlet serves the central pool for cells. The trapping channels radiate out from this central reservoir. The channels have alternating two posts and four posts respectively. Individual trapping regions for the cells can be addressed by the side channels. The fifth channel is curved to optimize the spacing between channel reservoirs. The device is designed to be coupled with MALDI-MS analysis of a target protein. Although this device has yet to be tested, it addresses most of the problems of the Generation-1 device.

## CHAPTER 5

### EXPERIMENTAL RESULTS AND DISCUSSION

Microfluidic platforms have become an important tool for single cell analysis as they are suitable to confine the pico, femto liter single cell analyte with minimal dilutions. Several studies have demonstrated the use of DEP to trap and manipulate analyte and relevant cell types such as cancer cells and bacteria. While single cell manipulation devices have been well demonstrated, the creation of a device capable of distinguishing a variety of different cell types with subsequent molecular studies on the single cell level is still a major challenge. The novel microfluidic device demonstrated, is used for trapping single particle and specifically single mammalian cancer cell types.

The assembled device (Figure 10) was tested for trapping single particles and single cancer cells. COMSOL simulations were performed with the devices and particle parameters to predict the trapping conditions using Eq. 21. The novel iDEP devices were applied for trapping single particles and single cancer cells. These devices were initially tested for trapping single polystyrene beads in different concentrations of phosphate buffer. The cells were trapped in a low conductivity buffer which reduced the Joule heating in the device. The DEP behavior of polystyrene beads was studied in varying concentrations of phosphate buffer. The beads express n-DEP and single bead trapping was observed with the ellipsoid device. Trapping of weakly metastatic mammalian breast cancer cells (MCF-7) was studied and compared to the trapping condition of the highly metastatic mammalian breast cancer cells MDA-MB-231 and mammalian PBMC. The

difference in dielectrophoretic behavior was exploited for selective trapping of the MCF-7 cancer cells from a mixture with PBMC and MDA-MB-231. A detailed study was conducted to determine the viability of the cells in the buffer and in the presence of the trapping electric field.

### **5.1 iDEP Trap for Single Particles (Polystyrene Beads)**

Polystyrene beads were used to test the microfluidic devices constructed for trapping single particles. The final devices were assembled and the single particle trap was constructed at the intersection of the four linear channels on a microfluidic platform as schematically depicted in Figure 9A). Potentials applied to each of the four channels can be controlled individually via electrodes immersed in the corresponding fluid reservoir as shown in Figure 9B). The trap is designed in such a way that it can also be used as an electrokinetic injector after the desired particle is trapped for further analysis. The behavior of the polystyrene beads was extensively studied and characterized [52], hence the devices were used to study the trapping behavior of the polystyrene beads. These preliminary studies were used to test the microfluidic devices.

Several experiments were performed with 10  $\mu\text{m}$  polystyrene beads and buffer media of varying conductivity (250  $\mu\text{S}/\text{cm}$  to 4  $\text{mS}/\text{cm}$ ) at a pH of  $6.8 \pm 0.2$ . The latex beads were coated with F108 in the corresponding buffer medium and 50 mL of the bead suspension was added to the inlet reservoir. All other channels were filled with the corresponding buffer without beads and reservoirs with 50 mL of this buffer.

### 5.1.1. Simulations

The trap designed for particles exhibiting n-DEP composed of one post with an elliptic base at the center of the intersection is shown in Figure 12. The geometries are designed for particles expressing n-DEP and p-DEP. Several structures were considered for the purpose of creating the optimized electric field for particle trapping. These posts were placed at the intersection of the two straight channels. The walls of the channel intersection were rounded to prevent undesired trapping region generation at those points. The two geometries considered for trapping are the ellipsoid post and tear drop posts as these geometries showed potential for trapping particles expressing n-DEP and p-DEP

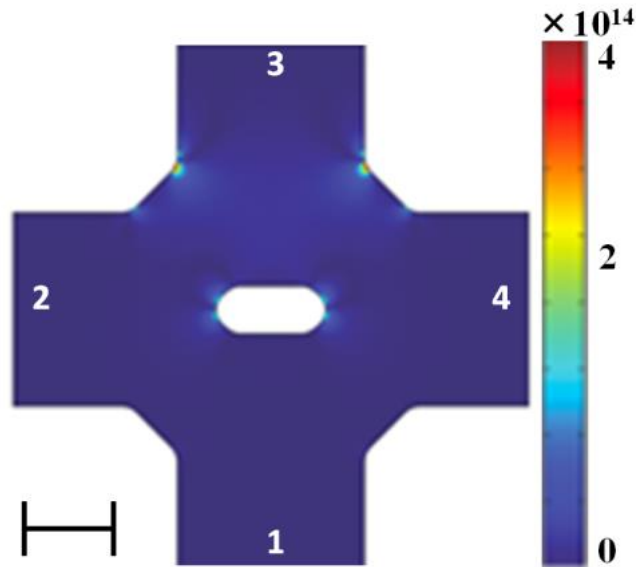


Figure 15: Numerical simulation of the electric field distribution. Computed  $\nabla E^2$  for the elliptic negative n-DEP single particle trap. The color scale showing  $\nabla E^2$  is in  $V^2/m^3$ . Positive potentials were applied to channels 1, 2, 3 and 4 corresponding to single particle trapping experiments. Scale bar is 40  $\mu m$ .

COMSOL Multiphysics software was used to compute the  $\nabla E^2$  values to reveal DEP trapping positions. The applied potentials at each reservoir (boundary) of the channel were adapted to match our experimental conditions (see figure legends). Particles with n-DEP behavior are expected to be repelled from the regions of higher electric fields and get trapped in areas of low field gradients. Figure 15 shows the distribution of  $\nabla E^2$  in the device with ellipsoid posts. Although  $\nabla E^2$  is the indicator for the trapping condition, the trapping behavior of the polystyrene particles was consistent at areas with low  $\nabla E^2$  values. The important aspect detected with this experiment is the dependency of the trapping potential on the concentration of the buffer used for trapping.

### **5.1.2. Experiments**

Negative DEP trapping of single particles was first studied with polystyrene beads. As previously reported by others [24, 70, 71], polystyrene particles exhibit a conductivity in the range of 2–10  $\mu\text{S}/\text{cm}$  as estimated from surface conductance measurements. It was thus assumed that negative CM factors were applicable for a conductivity range of the medium above 10  $\mu\text{S}/\text{cm}$ . Table 1 shows that indeed the CM factor is negative for all concentrations of phosphate buffer used in this study. The behavior of polystyrene beads in phosphate buffers of varying concentration and observed high bead adsorption to PDMS surfaces as well as particle aggregation was also studied. All microchannels were thus dynamically coated with the tri-block copolymer F108, effectively reducing the adsorption of microbeads to PDMS. This is in accordance

with the previously reported prevention of microbead adsorption by employing F108 as a coating agent in PDMS microfluidic devices [72, 73]. Furthermore, microbeads were pretreated in F108 solution overnight, which reduced bead aggregation effectively. Our trapping studies for polystyrene beads showed the expected negative trapping behavior at regions around the elliptical posts that exhibit the lowest  $\nabla E^2$  values.

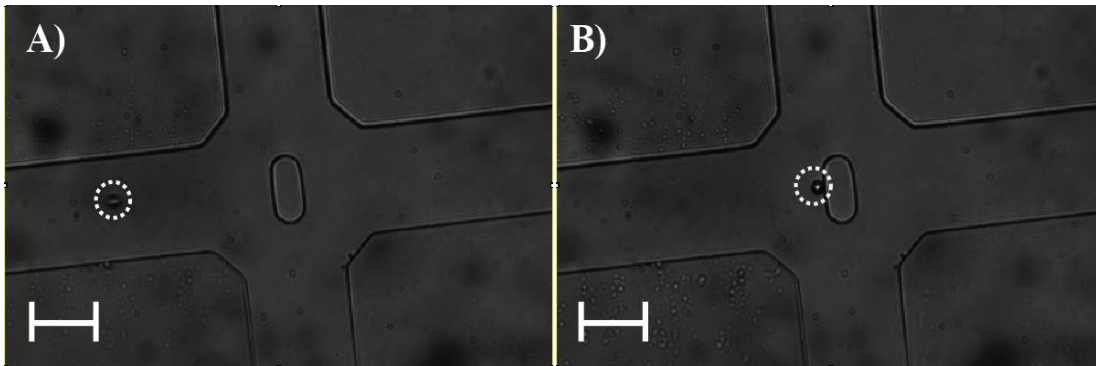


Figure 16: Snapshots of video sequences showing trapping of a single bead in the case of n-DEP with the elliptic trap design. (A) The bead travels toward the trapping position. (B) The bead is trapped in close agreement with the trapping position indicated through particle tracing with numerical simulations. Experiments were performed in phosphate buffer containing 1 mM F108. Potentials applied were 270 V at the inlet, -270 V at the outlet and 270 V at the side channels. Scale bar is 40  $\mu\text{m}$ . The pictures were obtained subsequently with a time difference of 200 ms between each frame.

As can be clearly seen from the image sequence in Figure 16, the bead is transported from the inlet toward the trap and immobilized at the inlet side of the elliptic post. Thus the proof-of-principle of a single particle trap in the case of n-DEP with the elliptic post design was demonstrated herein. The onset trapping electric field in which bead trapping first occurs dependent on the buffer conductivity was also investigated. For these experiments, phosphate buffers with conductivities from 0.3 to 4.9 mS/cm were

used. For each conductivity of the buffer used, the maximum value of the electric field ( $E_{\text{onset}}$ ) at which trapping was first observed in the trapping region was calculated with COMSOL simulations using the corresponding, experimentally determined potentials.

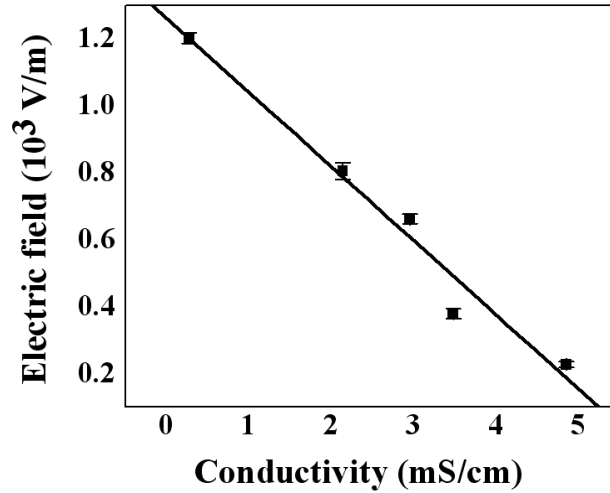


Figure 17: Shows the onset of the trapping electric field ( $E_{\text{onset}}$ ) versus conductivity of the buffer. The maximum field strengths were obtained by simulations with COMSOL using the applied potential in each channel at which trapping was observed adapted to the geometry used for numerical simulation. The line represents a linear fit as a guide to the eye. The error bars indicate the standard deviation obtained from  $n$  individual trapping experiments which varied between 20 and 30 for the five conductivity values tested.

**Table 2**

Buffer conductivity (mS/cm)	0.3	2.1	3.0	3.5	4.9
$f_{CM}$	-0.494	-0.499	-0.499	-0.499	-0.499

$f_{CM}$  factors of polystyrene beads for a particle conductivity of  $2\mu\text{S/cm}$

As demonstrated in Figure 17,  $E_{\text{onset}}$  decreased linearly with increasing medium conductivity. In the case of negative DEP, this could be caused by an increase in the CM factor according to a decrease in medium conductivity and concomitantly higher DEP

forces. However, Table 2 shows that the  $f_{CM}$  factor only decreases to a small extent in the conductivity range tested. On the other hand, DEP trapping is not the sole factor to be considered. The beads are transported via EOF into the trapping region and the resulting velocity profile will be dependent on both electroosmotic and DEP contributions. A decrease in electroosmotic flow is associated with increasing ionic strength [50, 74]. This explains that  $\mu_{EOF}$  is reduced and thus lower DEP forces are required to trap the beads within the higher conductivity buffers. As a consequence, the required trapping potential and thus the associated electric field is decreased with increasing concentration of the buffer medium. This dependence is in excellent agreement to the previously reported data with polystyrene particles [75].

## **5.2 iDEP Trap for Single Cancer Cells**

### **5.2.1 Single Cancer Cell Trapping (MCF-7) in HEPES/Glycerol Buffer**

The trap design investigated consists of two facing teardrop-shaped posts centered at the channel intersection. The  $\nabla E^2$  values were computed and are represented in Figure 18. For DEP purposes, typical cell media at high ionic concentrations was unsuitable as Joule heating effects arise which can destroy iDEP devices and harm the cells. Low conductivity buffers were thus used to keep heating effects at a minimum. In addition, it was necessary to maintain osmotically favorable conditions to prevent lysis of the cells. Therefore, HEPES buffer from 10-30 mM concentrations with 70–140 mM glycerol (maintaining the overall concentration at 100 or 150 mM) was employed. It is very

important to determine the viability of the cell population in the buffer containing HEPES and glycerol. For this, detailed viability tests were performed using this buffer with the two dyes ethidium homodimer 1 (EthD-1) and calcein (live/dead stain). Calcein is a non-fluorescent, hydrophobic compound that easily permeates active cell membranes.

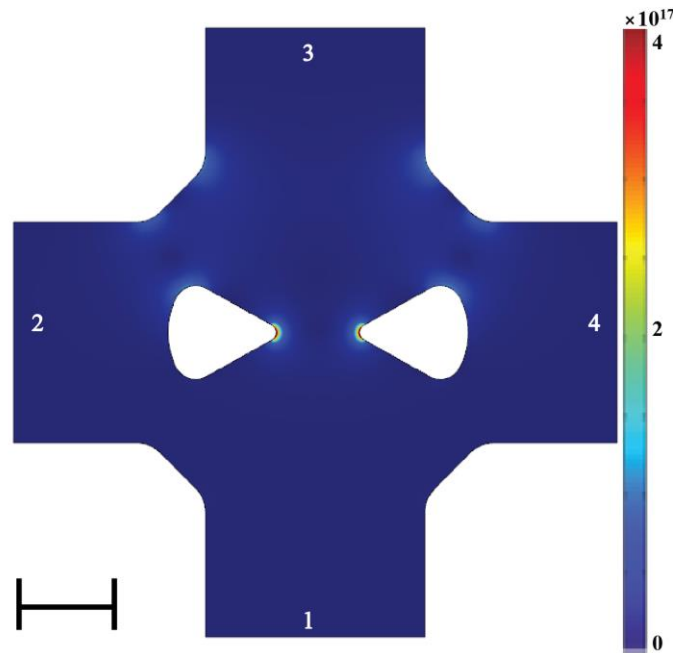


Figure 18: Numerical simulation of the  $\nabla E^2$  distribution for the tear-drop device. The color scale showing  $\nabla E^2$  is in  $\text{V}^2/\text{m}^3$ . Positive potentials were applied to channels 1, 2, 3 and 4 corresponding to single cell trapping experiments. Scale bar is 40  $\mu\text{m}$ .

Its hydrolysis by intracellular esterases produces a fluorescent compound that is retained within the cytoplasm. This dye produces an intense green fluorescence in live cells. The dye EthD-1 enters cells with compromised cell membranes and binds to the nucleic acid thereby producing an intense red fluorescence. This dye is excluded by the active membrane of live cells and thus serves as a stain for dead cells. The initial live/dead count of the obtained MCF-7 cells indicated that around 70% of the cells were alive, which represents the baseline for further viability assays (Figure 19). The MCF-7 cells

were then placed in a straight microfluidic channel in which an electric field of 100 V/cm was applied for two or four minutes. Subsequently, the cell viability was assessed after live/dead staining.

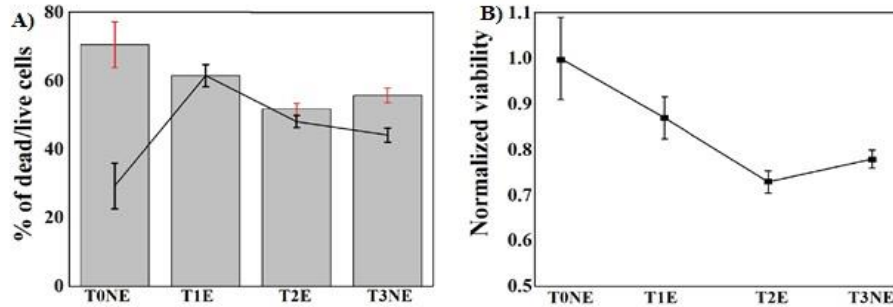


Figure 19: (A) Effects of electric fields on MCF-7 cancer cell viability. Column bars indicate live cell population distribution; trend line indicates dead cell population distribution. The viability of MCF-7 cells in HEPES/glycerol (70 mM/30 mM) buffer was assessed with live/dead staining after application of an electric field for two (T1) and four (T2) minutes. In addition the viability was measured after 45 min (T3) without the application of an electric field (no electric field, NE). (B) Relative viability of the MCF-7 cells. Between 110 and 150 cells were counted for each condition. The error bars indicate the standard deviation from three independent experiments.

As shown in Figure 19, the cell viability was not affected significantly by the application of the electric field for 2 min (two-tailed Student's t-test, probability value  $p > 0.1$ , not significant, with  $n = 3$ ). This corresponds to roughly the average length of a single experiment (~90 s). Only after continuing the application of the electric field for 4 min, a significant loss of viability was observed (two-tailed Student's t-test, probability value  $p < 0.01$ , significant, with  $n = 3$ ). As a control, cells were incubated at room temperature for 45 min corresponding to the overall immersion time in the HEPES/glycerol buffer including the control experiment at the start and all data acquisition times between electric field applications. This control experiment also

resulted in a reduction of live cells to a similar extent as the application of an electric field for 4 min. Our results thus indicate that iDEP manipulation of viable MCF-7 cells is feasible and that a single experiment should be concluded within two minutes to avoid damage to the cells. It should also be remarked that the dead cell count after 4 min is in the same range as the viability after immersion in the buffer system for 45 min indicating that the decrease in the dead/live cell count is also affected by the HEPES/glycerol buffer over longer time periods.

Trapping of the MCF-7 cancer cells was then performed with cells suspended in 30 mM HEPES and 70 mM glycerol buffer in experiments where the tear drop device was used for trapping. It is important to notice that this trap was designed for single cells with a maximum diameter of 20  $\mu\text{m}$  such that the gap in-between the two posts was large enough to prevent geometrical trapping. Figure 20 shows an image sequence of the trapping of a single cell injected from the inlet side.

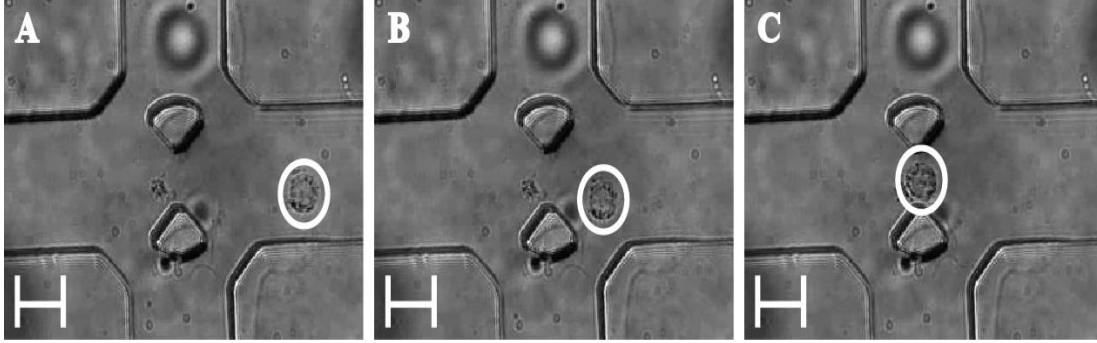


Figure 20: Snapshots of video sequences showing trapping of a single MCF-7 cell for p-DEP with the teardrop trap design. (A) The cell travels toward the trapping position. (B) The cell is directed toward the tips of the teardrop posts. (C) The cell is trapped by iDEP in close agreement with numerical simulations. Potentials applied were +100 V at the inlet, -100 V at the outlet and +100 V at the side channels. Scale bar is 20  $\mu\text{m}$ . Imaging was performed at a frame rate of 200 ms/frame. Images (A) and (B) correspond to frames 1 and 2, respectively, whereas (C) corresponds to frame 4 in chronological order.

The cell is transported toward the trap and captured at the center region of the teardrop trap after application of a potential of +100 V at the inlet, -100 V at the outlet and +100 V at the side channels. The cells were kept trapped for about a minute before dropping the potential in order to ensure that it was not just transient adhesion to the posts. Furthermore, it was demonstrated that iDEP can be successfully employed for trapping of individual cancer cells. In the experiments, an average of six attempts was required before a single cell could be trapped.

### 5.2.2 Single Cancer Cell Trapping (MCF-7) in HEPES/Trehalose Buffer

The buffer consisting of 30 mM HEPES with 120 mM Trehalose was used for the trapping experiment, thereby maintaining the overall concentration of the buffer at 150

mM. The conductivity of the buffer ranged from 10-12  $\mu\text{S}/\text{cm}$  with a pH of 5.1.

Trapping experiments were performed with the MCF-7 cells in the tear-drop device.

Figure 21 shows an image sequence for the trapping of a single cell injected from the inlet side. The cell is transported toward the trap and captured at the center region of the tear-drop trap after application of a potential of -10 V at the inlet +90 V at the outlet and -10 V at the side channels. The cells were kept trapped for about a minute before dropping the potential in order to ensure that it was not just transient adhesion to the posts.

Tests were performed with the cells using Calcein-AM and Ethidium homodimer-1 dye to determine the viability of the cells in the buffer medium. To further substantiate the viability of employed cells under iDEP trapping conditions, viability tests were

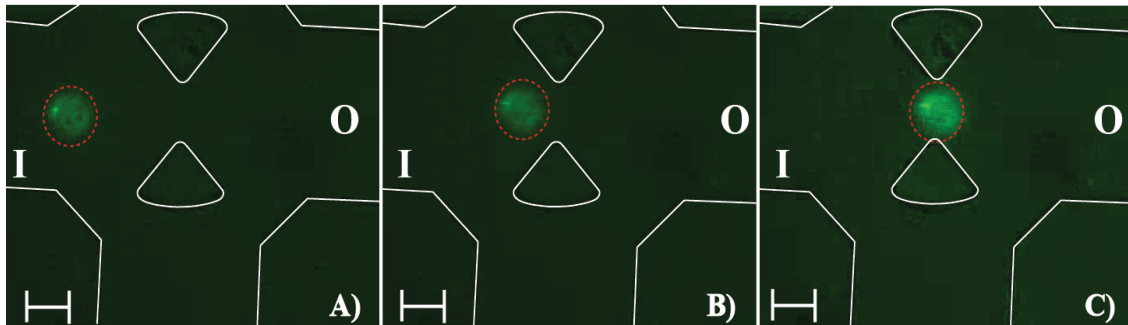


Figure 21: Snapshots of video sequences showing trapping of a single live MCF-7 cell for DEP with the teardrop trap design. (A) The cell travels toward the trapping position. (B) The cell is directed toward the tips of the teardrop posts. (C) The cell is trapped by iDEP in close agreement with numerical simulations. Potentials applied were -10 V at the inlet, -90 V at the outlet and -10 V at the side channels. Scale bar is 20  $\mu\text{m}$ . Imaging was performed at a frame rate of 200 ms/frame. Images (A) and (B) correspond to frames 1 and 2, respectively, whereas (C) corresponds to frame 5.

conducted on larger cell numbers (~100) within the microfluidic device without potentials applied and under trapping conditions.

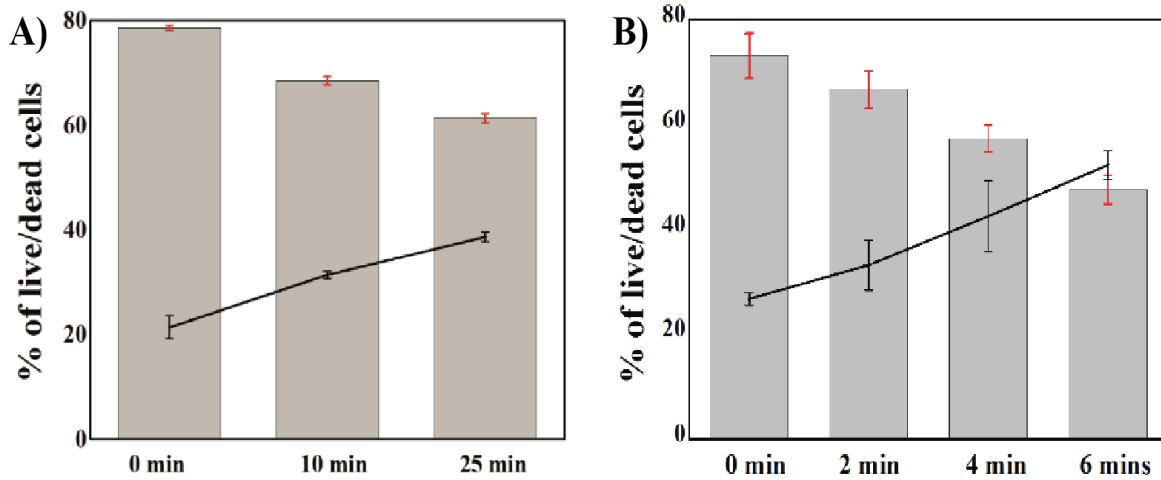


Figure 22: Viability of MCF-7 cells population in HEPES/trehalose buffer of 30 mM/120 mM concentrations. Imaging was performed with Calcein-AM and EthD-1 dye. Column bars indicate population of live cells and the trend line shows the population of dead cells. (A) Shows population distribution of the cells suspended in the buffer solution. (B) Shows distribution of cell population with the application of 100 V/cm electric field.

The initial live/dead cell assay indicated that 78.6% of the MCF-7 cell population was viable as demonstrated in Figure 22A, which represents the baseline for the viability studies. The cells were incubated in the viability test buffer for a total of 45 min and populations were imaged at intervals of 10 and 25 min. After 25 min, 61.4% of the MCF-7 cell population was still viable. This test demonstrated that incubation times below 25 min do not considerably decrease the viable cell population. Note that in the microfluidic single cell trapping experiments presented herein; cell populations were replenished after 30 minutes to avoid cell populations with significant amounts of dead cells.

It is also important to examine the influence of the applied electric field on cell viability. Upon application of potentials corresponding to trapping conditions for MCF-7 to a test channel, cell populations were imaged every 2 min for a total of 6 min. As demonstrated in Figure 22B, at the end of applying a potential for 2 min, 68.5% of the MCF-7 cell population remained viable. Compared to the MCF-7 cell population, the live population of B-lymphocytes decreased more rapidly under electric field application. It was suspected that the faster decrease in viable cells under the application of an electric field compared to conditions without applied electric field could originate from the combined effect of the buffer system coupled with the application of an electric field. However, note that the duration of electric field application in a single cell trapping experiments never exceeded 2 min. These results indicate that iDEP manipulation of live cells can be successfully conducted provided that the duration of the experiment is on the order of 2 min.

### **5.3 Single Cancer Cell Trapping (MDA-MB-231) in HEPES/Trehalose Buffer**

#### **5.3.1 Experiments**

Breast cancer cells can be distributed along a spectrum of differentiation from epithelial to mesenchymal appearances [76-78]. On the basis of the phenotype and invasiveness, the breast cancer cell lines can be classified into three categories. The first category consists of cells that express a high amount of markers like estrogen receptor alpha (ER alpha) and E-cadherin molecules, which are typical of a more epithelial

phenotype and MCF-7 cells. The second category resembles the first category of cells but contains cells that show a weakly epithelial phenotype with a low expression of epithelial biomarkers. The third category of breast cancer cells is highly invasive *in vitro* with a mesenchymal phenotype. These cell types, including MDA-MB-231, also express high levels of a marker typically found in mesenchymal cells [79]. Cells of the mesenchymal phenotype have strong migratory and invasive abilities attributing a higher degree of metastatic potential to the MDA-MD-231 cells.

The transition from an epithelial to a mesenchymal phenotype can be characterized by changes in expression levels of various proteins [79]. For example, the increased expression of vimentin and loss of epithelial cell adhesion molecules like E-cadherin and ER alpha are reported as biomarkers for the transition from the epithelial to mesenchymal phenotypes [79]. Indeed, it has been demonstrated that human breast cancer progression first results in the loss of ER alpha and subsequent expression of vimentin, the latter being associated with increased metastatic potential through enhanced invasiveness [77]. It is therefore necessary to observe the difference in trapping behavior of these two categories of cancer cells. The highly invasive MDA-MB-231 cells were chosen for iDEP trapping experiments with the tear-drop device in the HEPES/trehalose buffer. The conductivity of the buffer ranged from 10-12  $\mu\text{S}/\text{cm}$  with a pH of 5.1. Figure 23 shows an image sequence of the trapping of a single MDA-MB 231 cell injected from the inlet side.

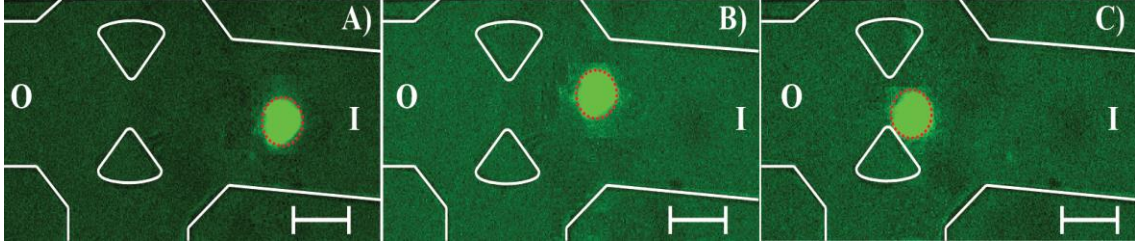


Figure 23: Snapshot video sequence showing trapping of a single live MDA-MB-231 cell *via* n-DEP with the teardrop design. (A) The cell travels toward the trapping position. (B) The cell is directed towards the tip of the teardrop posts. (C) The cell is trapped by n-DEP in close agreement with numerical simulations. Potentials applied were -10 V at the inlet, -190 V at the outlet and -10 V at the side channels. Scale bar is 20  $\mu\text{m}$ . Imaging was performed at frame rate of 200 ms/frame. Images (A) and (B) correspond to frames 1 and 2 respectively, whereas (C) is frame 5.

The cell is transported toward the trap and captured at the center region of the teardrop trap after application of a potential of -10 at the inlet, -190 V at the outlet and -10 V at the side channels. The cells were kept trapped for about a minute before dropping the potential in order to ensure that it was not just transient adhesion to the posts. This trapping behavior is substantially different from that of the weakly metastatic MCF-7 cells, which were trapped at 100 V/cm in the same device with the same buffer. The differential trapping behavior is exploited for selective trapping of the MCF-7 cells from the mixture with MDA-MB-231 cells.

### 5.3.2 Simulations

It is important to determine the condition suitable for trapping the single cancer cell in the devices. COMSOL Multiphysics software was used to identify the condition where the trapping condition (Eq. 21) was met for the MDA-MB-2231 cells with  $\mu_{DEP}$  of  $1.04 \times 10^{-17} \text{ m}^4/\text{V}^2 \cdot \text{s}$  and  $\mu_{EOF}$  of  $2.52 \times 10^{-9} \text{ m}^2 \text{ V}^{-1} \text{ s}^{-1}$ , as determined experimentally. This

gives an overview of the possible trapping regions and the trapping behavior of the cells. As demonstrated in Figure 24, with an applied potential of  $-0.1\text{V}$  at the inlet and side channels and  $-1.90\text{V}$  at the outlet, the trapping condition is met for the MDA-MB-231 cells with values of Eq. 21 larger than 1 up to a maximum of 5 at the teardrop posts.

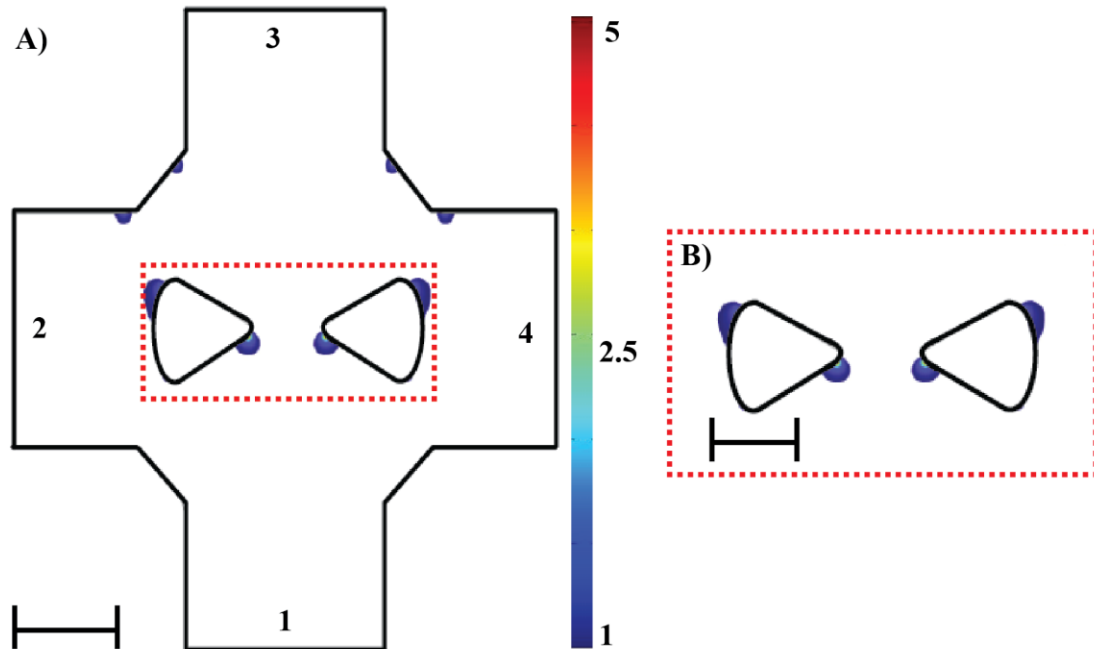


Figure 24: Simulation of the tear-drop device with trapping conditions for MDA-MB-231 cells. Potentials were applied to 1, 2, 3 and 4 according to trapping experiment. (A) Shows simulation of complete intersection. Scale bar is  $40\ \mu\text{m}$ . (B) Shows tear-drop posts. Color scale bar indicates region where trapping condition is greater than one. Scale bar is  $20\ \mu\text{m}$ .

Simulations were repeated with trapping potentials where MDA-MB-231 cells were captured, however, using parameters for MCF-7 cells, obtained values for Eq. 24 were compared in the regions where the trapping condition of unity was previously found for MCF-7. Since the resulting values were larger than unity at the MDA-MB-231

trapping potential, Eq. 22 was normalized to unity to find the corresponding  $\mu_{DEP}$  for MDA-MB-231 cells. This  $\mu_{DEP}$  value for MDA-MB-231 was further used to determine the  $f_{CM}$  using Eq. 24 and subsequently  $\sigma_p$  was determined as well. The single shell model was used to determine  $\sigma_{mem}$  using Eq. 24.

### 5.3.3 Viability Study

To substantiate the viability of employed cells under iDEP trapping conditions, viability tests were conducted on larger cell numbers (~100) within the microfluidic device without potentials applied and under trapping conditions.

The initial live/dead cell assay indicated that 73.2% of the MDA-MB-231 cells were viable as demonstrated in Figure 25A, which represents the baseline for the viability studies. The cells were incubated in the viability test buffer for a total of 45 min and populations were imaged at intervals of 10 and 25 min. After 25 min, 54.2% of the MDA-MB-231 population was alive. This test demonstrated that incubation times below 25 min do not considerably decrease the viable cell population. During the single cell trapping experiments in the microfluidic device, cell populations were replenished after 30 minutes to avoid cell populations with a significant amount of dead cells.

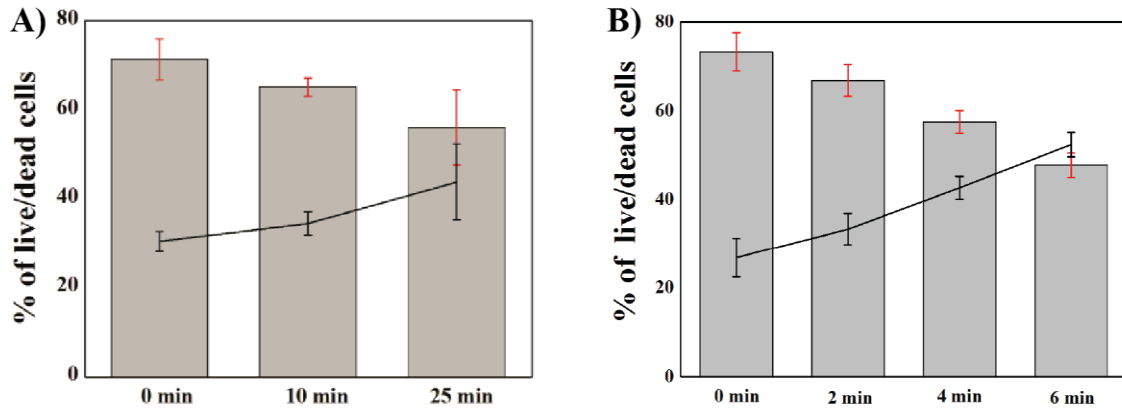


Figure 25: Viability of MDA-MB-231 cells population in HEPES/trehalose buffer of 30 mM/120 mM concentration. Imaging was performed with Calcein-AM and EthD-1 dye. Column bars indicate the population of live cells and the trend line shows population of the dead cells. (A) Shows the population distribution of the cells suspended in the buffer solution. (B) Shows the distribution of the cell population with the application of a 200 V/cm electric field.

It is also important to examine the influence of the applied electric field on cell viability. Upon application of potentials corresponding to trapping conditions for MDA-MB-231 to a test channel, cell populations were imaged every 2 min for a total of 6 min. As demonstrated in Figure 25B, at the end of applying a potential of 200 V/cm for 2 min, 66.7% of the MDA-MB-231 cell population remained viable. After 6 min, the viable cell count decreased to 47.6%. Electric field application in a single cell selective trapping experiment never exceeded 2 min. These results indicate that iDEP manipulation of live MDA-MB-231 cells can be successfully conducted provided that the duration of the experiment is on the order of 2 min. Furthermore, the trapping condition of the MCF-7 cells under the buffer conditions in the tear-drop trapping device was determined to be 200 V/cm. This is different from the trapping condition of the MCF-7 cells under the same buffer conditions and in the same tear-drop device.

#### **5.4 Single Cell Trapping of Peripheral Blood Mononuclear Cells (PBMC) in HEPES/trehalose Buffer**

Understanding the DEP characteristics of different cell types can be beneficial for performing selective cell trapping. Characterizing the DEP response of cells with varying radii is also important in understanding the variation of DEP properties with respect to cell size. Dielectrophoretic properties of particles vary greatly with their radius. PBMC cells, which are important constituent of whole blood, are chosen as a model sample to study the trapping behavior of these cells in the HEPES/trehalose buffer using the tear-drop device. These cells are characterized by large round nuclei and small radii. The population of PBMC used for the study consisted of B-lymphocytes, T-lymphocytes and natural killer (NK) cells. The conductivity of the buffer ranged from 10-12  $\mu\text{S}/\text{cm}$  with a pH of 5.1. The cell is transported toward the trapping region at the center of the tear-drop trap after application of an electric field from 100 V/cm to 1300 V/cm. No trapping of the PBMC was observed in this range. Electric field application above 1300 V/cm damaged the device and generated air bubbles in the device affecting performance.

To further substantiate the viability of employed cells under iDEP trapping conditions, viability tests were conducted using larger cell numbers (~100) within the microfluidic device without potentials applied and under trapping conditions. The initial live/dead cell assay indicated that 70.9% of the PBMC population and was viable as demonstrated in Figure 26, which represents the baseline for the viability studies. The cells were incubated in the viability test buffer for a total of 45 min and populations were imaged at intervals of 10 and 25 min. After 25 min, 43.9% of the B-lymphocyte

population was alive. This test demonstrated that incubation times below 25 min do not considerably decrease the viable cell population. This limits the application of the cell population to 30 min. The cell population for the single cell trapping experiments was replenished after 30 min to avoid cell populations with a significant amount of dead cells.

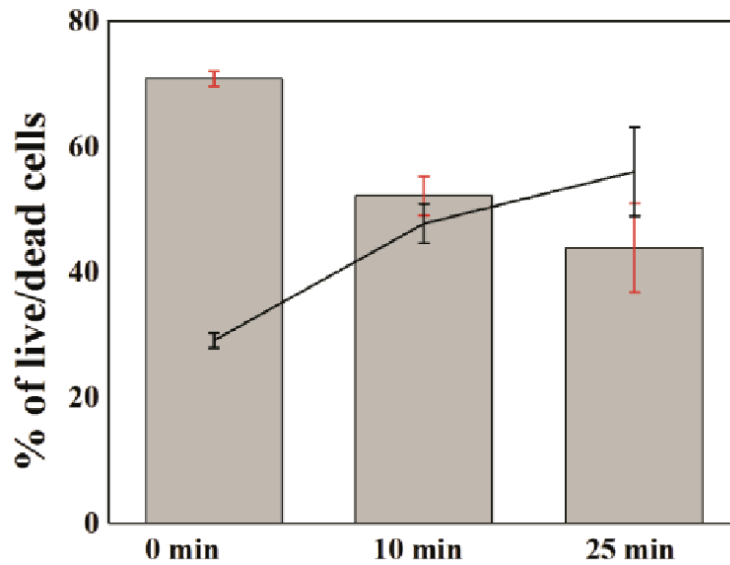


Figure 26: Shows the viability of the PBMC population in HEPES/trehalose buffer of 30 mM/120 mM concentrations, respectively. Imaging was performed with Calcein-AM and EthD-1 dye. Column bars indicate the population of live cells and the trend line shows the population of the dead cells.

### 5.4.1 Selective trapping of MCF-7 and PBMC

MCF-7 cells are weakly metastatic mammalian breast cancer cells. PBMC are normal cells, but are a major constituent of the blood. MCF-7 cells are much larger than PBMC, therefore they have different DEP trapping behavior. To further substantiate this differential trapping behavior, selective trapping experiments were conducted. The trapping condition of the weakly metastatic MCF-7 cancer cells was different from the PBMCs in the same buffer conditions with the tear drop device. The MCF-7 cells were trapped at 100 V/cm in the tear-drop device, while the PBMC were not trapped under this condition in the same device. To test selective trapping experimentally, MCF-7 and PBMCs were suspended together in the working buffer of HEPES (30mM) and trehalose (120mM). Figure 27 shows an image sequence demonstrating the selective trapping of MCF-7 cells in the intersection region of the iDEP trap and a mobile PBMC flowing through the trapping area and away from the trapped MCF-7 cell.

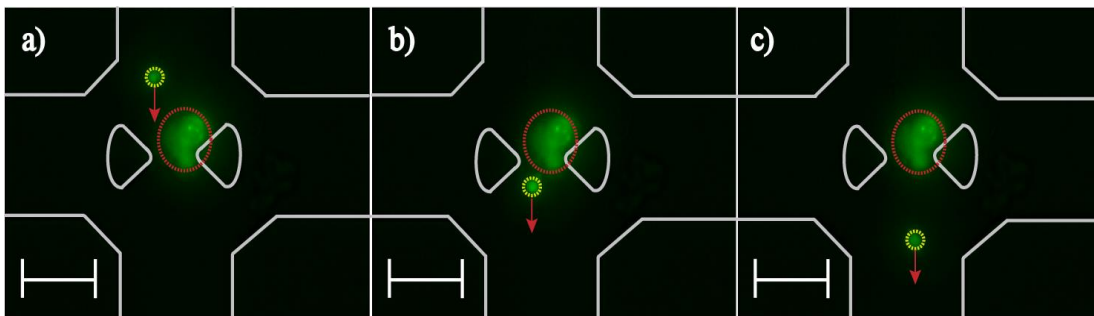


Figure 27: Snapshots depicting a selective trapping sequence for MCF-7 and PBMC. A viable MCF-7 cell is trapped between the tips of teardrop posts, while the smaller B-lymphocyte flows through the trapping region. (a) Snapshot of a trapped MCF-7 cell with PBMC arriving at the iDEP trap. (b) PBMC flowing through trapping region. (c) PBMC after the trapping region. Individual cells are outlined by red (MCF-7)

and yellow (PBMC) contour lines. The time between image (a) and (b) was 1 s and between (b) and (c) was 0.8 s. Scale bar is 50  $\mu\text{m}$ .

## 5.4.2 Simulations

COMSOL Multiphysics software was used to identify where the trapping condition (Eq. 21) was met for the MCF-7 cells with  $\mu_{DEP}$  of  $-2.22 \times 10^{-17} \text{ m}^4/\text{V}^2 \cdot \text{s}$  and  $\mu_{EOF}$  of  $2.52 \times 10^{-9} \text{ m}^2 \text{ V}^{-1} \text{ s}^{-1}$ . This selective trapping of single MCF-7 cells is observed when -50 V is applied at the outlet and 50 V at the inlet and side channel reservoirs. Note that this potential was determined by a successive increase of potentials in all reservoirs in 10 V steps until iDEP trapping was observed for individual MCF-7 cells. The experimental observation is in excellent agreement with the numerical simulations (Figure 28) of the trapping condition with cell DEP properties reported by Hu *et al.* [80] and Bordi *et al.* [81]. The values associated with the DEP trapping behavior of the cells are given in Table 2.

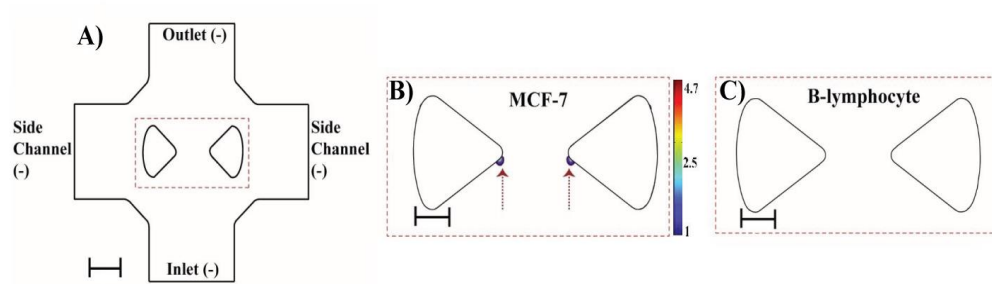


Figure 28: (A) Schematic of the iDEP device describing the inlet, outlet and two side channels, (B-C) Simulation of the trapping condition Eq. 21 and zoom in corresponding to the region marked in red (C) for MCF-7, (C) PBMC with potentials of 50V at inlet and side channel reservoirs and -50V at outlet reservoir. See text for detailed simulation conditions.

The corresponding DEP properties of B-lymphocytes do not suggest trapping, since the trapping condition was not fulfilled in the theoretical modeling (Figure 28) in accordance with the experimental observation. Comparison of  $f_{CM}$ ,  $\mu_{DEP}$ ,  $\sigma_p$  and  $\sigma_{mem}$  for the different types of cells in PBMC and MCF-7 is given in Table 3. The difference in the  $\mu_{DEP}$  values of the different cells is mainly due to the difference in size of the cells. This proves that the device can be used for selective trapping of the target cell.

The green fluorescence of both trapped MCF-7 cells and PBMC in our study reveal selective single cell trapping of viable cells. To further substantiate the viability of employed cells under iDEP trapping conditions, viability tests were conducted on a larger number of cells (~100) within the microfluidic device without potentials applied and under trapping conditions as shown in Figure 29.

**Table 3**

Cell Type	$R_{tot}$ ( $\mu\text{m}$ )	$t_{mem}$ ( $\mu\text{m}$ )	$\sigma_{mem}$ (S/m)	$\sigma_{cyto}$ (S/m)	$\sigma_{p,1shell}$ (S/m)	$f_{CM}$	$\mu_{DEP}$ ( $\text{m}^4/\text{V}^2 \cdot \text{sec}$ )
MCF-7	15	$7.0 \cdot 10^{-3}$ (h)	$1 \cdot 10^{-6}$ (b)	1.0 <sup>(i)</sup>	$30.82 \cdot 10^{-4}$ (e)	-0.41 <sup>(d)</sup>	$-2.22 \cdot 10^{-17}$ (c)
B-lymphocyte	2.9 <sup>(a)</sup>	$7.5 \cdot 10^{-3}$ (a)	$8.0 \cdot 10^{-5}$ (a)	0.6 <sup>(a)</sup>	$293.16 \cdot 10^{-4}$ (e)	0.02 <sup>(d)</sup>	$5.51 \cdot 10^{-20}$ (c)
T-lymphocyte	2.8 <sup>(a)</sup>	$7.5 \cdot 10^{-3}$ (a)	$2.7 \cdot 10^{-5}$ (a)	0.6 <sup>(a)</sup>	$98.84 \cdot 10^{-4}$ (e)	-0.26 <sup>(d)</sup>	$-4.95 \cdot 10^{-19}$ (c)
NK Cells	7.5 <sup>(f)</sup>	N/A	N/A	N/A	N/A	N/A	$-4.12 \cdot 10^{-18}$ (g)

(a) From [81], (b) From [82], (c) From Eq. 15, (d) From Eq. 5, (e) From Eq. 24, (f) From [83], (g) From Eq. 15 using  $f_{CM}$  value of T-lymphocytes,

The initial live/dead cell assay indicated that 78.6% of the MCF-7 cell population and 70.9% of the PBMC population are viable without application of electric field, as demonstrated in Figure 22A and 26. which represents the baseline for the viability studies. This test also demonstrated that incubation times below 25 min do not considerably decrease the viable cell population. Note that in the microfluidic single cell trapping experiments presented herein, cell populations were replenished after 30 min to avoid cell populations with a significant amount of dead cells.

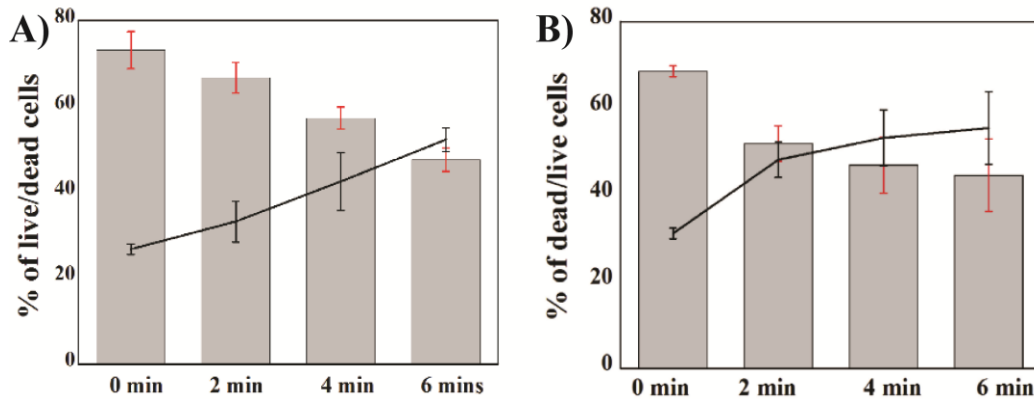


Figure 29: Viability of MCF-7 cells and PBMC were probed over various time intervals with application of an electric field of 100 V/cm, corresponding to the trapping condition. (A) Shows the viability distribution of MCF-7. (B) Shows viability distribution of PBMC. Imaging was performed with Calcein-AM and EthD-1 dye. Column bars indicate the population of live cells and the trend line shows the population of dead cells

It is also important to examine the influence of the applied electric field on cell viability. Upon application of potentials corresponding to trapping conditions for MCF-7 to a test channel, cell populations were imaged every 2 min for a total of 6 min. As demonstrated in Figure 29, at the end of applying potential for 2 min, 68.5% of the MCF-7 cell population and 51.8% of the PBMC population remained viable. Compared to the

MCF-7 cell population, the live population of PBMC decreased more rapidly under electric field application. After 6 min, the viable cell count (44.5%) decreased to less than the amount of dead cells (55.4%). However, the MCF-7 cells were more robust since viable cells were still slightly dominating after the treatment. It was suspected that the faster decrease in viable cells under the application of an electric field compared to conditions without electric field applied could originate from a combined effect of the buffer system coupled with the application of an electric field. However, note that the duration of electric field application in a selective single cell trapping experiment never exceeded 2 min. These results indicate that iDEP manipulation of live cells can be successfully conducted provided that the duration of the experiment is on the order of 2 min.

## **5.5 Selective Trapping of MCF-7 and MDA-MB-231**

MDA-MB-231 cells which are transfected with the fluorescent protein dTomato were used for the selective trapping experiments. MCF-7 cells were labeled with Calcein-AM stain only.

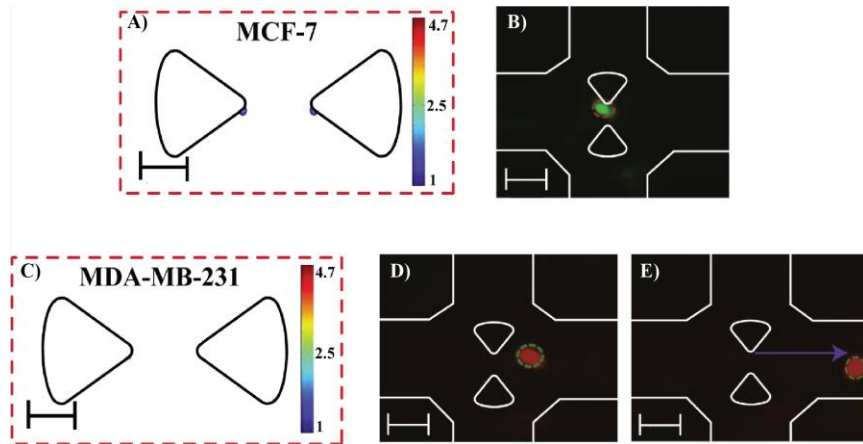


Figure 30: Trapping conditions and snapshots depicting a selective trapping sequence for MCF-7 and MDA-MB-231. (A) Trapping area and trapping condition for MCF-7 as obtained from Eq. 21 and conditions explained in the main text. (B) Snap shot of a trapped MCF-7 cell. (C) Trapping area and trapping condition for MDA-MB-231. (D)-(E) Snap shot sequence of MDA-MB-231 flowing through the trapping region under experimental conditions of -10V inlet and side channel reservoirs and -190V outlet reservoir, in which trapping was observed for MCF-7 cells.

This differential enabled the ability to distinguish the two types of cells exhibiting comparable size. As demonstrated previously, the trapping condition of MCF-7 cells was different from the MDA-MB-231 cells in the same buffer conditions. The MCF-7 cells were trapped at 100 V/cm in the tear-drop device, while the MDA-MB-231 cells were trapped at 200 V/cm under the same buffer conditions and in the same device. To test selective trapping experimentally, MCF-7 and PBMCs in the working buffer of HEPES (30mM) and trehalose (120 mM) were first employed. Figure 30 shows an image sequence demonstrating the selective trapping of MCF-7 cells in the intersection region of the iDEP trap and a mobile MDA-MB-231 flowing through the trapping area. This demonstrates selective trapping of MCF-7 in a mixture with MDA-MB-231 cells using the tear drop device.

### 5.5.1 Simulations

COMSOL Multiphysics software was used to identify the condition where the trapping condition (Eq. 21) was met for the MCF-7 cells. This selective trapping of single MCF-7 cells is observed when -10 V is applied at the inlet as well as side channels and -190 V at the outlet reservoir. Note that this potential was determined by a successive increase of potentials in all reservoirs in -10 V steps until iDEP trapping was observed for individual MCF-7 cells. The experimental observation is in excellent agreement with the numerical simulations shown in Figure 30 A and C. The corresponding DEP properties of MDA-MB-231 do not suggest trapping since the trapping condition was not fulfilled in the theoretical modeling (Figure 31 C) in accordance with the experimental observation. Comparison of  $f_{CM}$ ,  $\mu_{DEP}$ ,  $\sigma_p$  and  $\sigma_{mem}$  for the MCF-7 and MDA-MB-231 is given in Table 4.

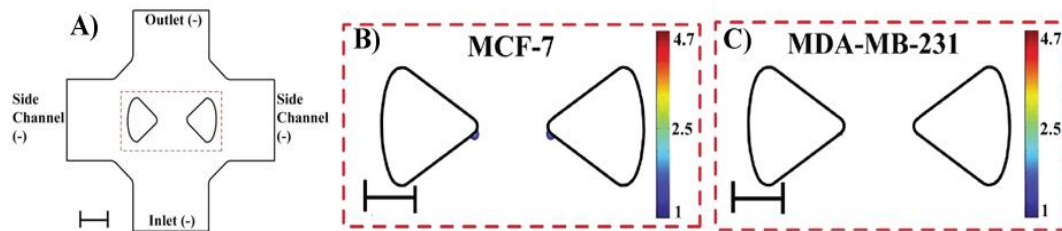


Figure 31: (A) Schematic of iDEP device describing the inlet, outlet and two side channels, B-C) Simulation of the trapping condition (Eq. 21) and zoom in corresponding to the region marked in red (B) for MCF-7, (C) MDA-MB-231 with potentials of 10V at inlet and side channel reservoirs and -190V at outlet reservoir. See text for detailed simulation conditions.

**Table 4****Input Values of MCF-7 and MDA-MB-231 Used for Numerical Simulations.**

Cell Type	$R_{tot}$ ( $\mu\text{m}$ )	$t_{mem}$ ( $\mu\text{m}$ )	$\sigma_{mem}$ (S/m)	$\sigma_{cyto}$ (S/m)	$\sigma_{p,1shell}$ (S/m)	$f_{CM}$	$\mu_{DEP}$ ( $\text{m}^4/\text{V}^2\text{sec}$ )
MCF-7	15	$7.0 \cdot 10^{-3(e)}$	$1 \cdot 10^{-6(a)}$	$1.0^{(f)}$	$30.82 \cdot 10^{-4(d)}$	$-0.41^{(c)}$	$-2.22 \cdot 10^{-17(b)}$
MDA-MB-231	15	NA	$0.9 \cdot 10^{-6(g)}$	NA	$1.37 \cdot 10^{-4(d)}$	$-0.19^{(b)}$	$-1.04 \cdot 10^{-17(h)}$

(a) From [82], (b) From Eq. 15, (c) From Eq. 24, (d) From Eq. 23, (e) From [80], (f) From [84], (g) From Eq. 23 with  $\sigma_{cyto}$ ,  $t_{mem}$  and  $R_{tot}$  for MCF-7, (h) From Eq. 15 (see text)

To further substantiate the viability of employed cells under iDEP trapping conditions, viability tests were conducted using larger numbers of cells (~100) inside the microfluidic device under the trapping conditions shown in Figure 32. The initial live/dead cell assay indicated that 78.6% of the MCF-7 cell population and 73.2% of the MDA-MB-231 population was viable as demonstrated in Figure 22A and 25A, which represents the baseline for the viability studies. This test also demonstrated that incubation times below 25 min do not considerably decrease the viable cell population. Note that in the microfluidic single cell trapping experiments presented herein, cell populations were replenished after 30 minutes to avoid cell populations with a significant amount of dead cells.

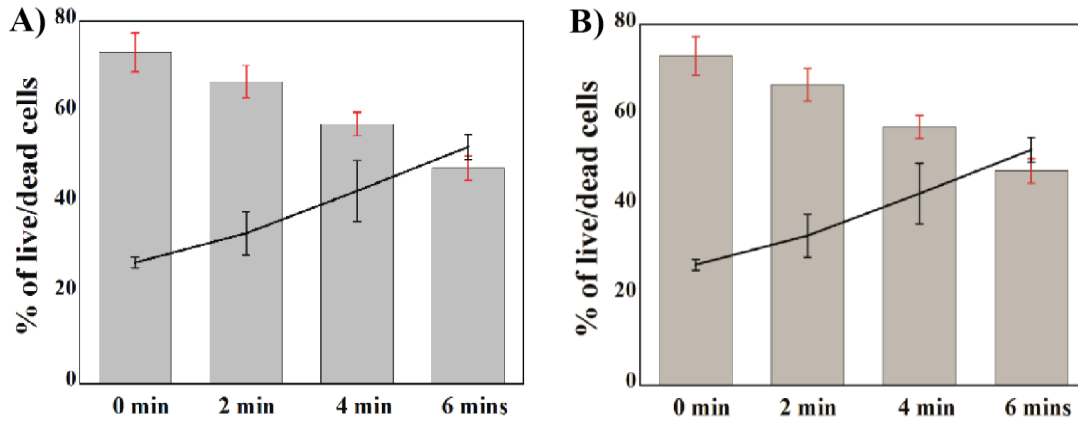


Figure 32: Viability of MCF-7 and MDA-MB-231 cells were probed over various time intervals with application of an electric field of 100V/cm, corresponding to the trapping condition. The trend line in the plot describes the dead cell population. (A) Shows the viability distribution of MCF-7 cells. (B) Shows the viability distribution of MDA-MB-231 cancer cells. Imaging was performed with Calcein-AM and EthD-1 dye. Column bars indicate the population of live cells and the trend line shows the population of the dead cells.

It is also important to examine the influence of the applied electric field on cell viability. Upon application of potentials corresponding to trapping conditions of 100 V/cm for MCF-7 to a test channel, cell populations were imaged every 2 min for a total of 6 min.

As demonstrated in Figure 32, at the end of applying a potential of 100V/cm for 2 min, 68.5% of the MCF-7 cell population and 63.4% of the MDA-MB-231 cell population remained viable. It is suspected that the faster decrease in viable cells under the application of an electric field compared to conditions without electric field applied could originate from the combined effect of the buffer system coupled with the application of an electric field. However, note that the duration of electric field application in a selective single cell trapping experiment never exceeded 2 min. These results indicate that iDEP

manipulation of live cells can be successfully conducted provided that the duration of the experiment is on the order of 2 min.

## **5.6 Importance of Differential Trapping of MCF-7 and MDA-MB-231**

Since this study was conducted under DC conditions, the frequency related capacitance changes leading to dielectrophoretic property variations cannot be applied to distinguish various cell types. However, these experiments showed distinctive iDEP trapping potentials for all three cell types. While for PBMCs variations in trapping potentials can be attributed to the significantly smaller radius of B- and T-lymphocytes as well as NK cells compared to the two breast cancer cells, the differences in observed trapping behavior of the two cancer cell lines may be related to their metastatic potential as described previously.

## CHAPTER6

### CONCLUSION

This work has demonstrated a novel method to trap individual particles and single cancer cells using iDEP in a microfluidic device. Numerical simulations were performed to reveal the electric field distribution at the trapping zone and fabricated iDEP devices in PDMS were used to perform experiments for particles exhibiting negative DEP behavior. The proof-of-principle of this novel single particle trapping strategy was demonstrated by trapping single 10  $\mu\text{m}$  diameter polystyrene beads exhibiting negative DEP in a simple geometry. It was also found that the onset of trapping decreased with an increase in the buffer conductivity, which is attributed to the reduction in electroosmotic flow and thus increased DEP trapping. For iDEP trapping of cancer cells, the buffer medium conditions were optimized and it was found that MCF-7 cells remained viable in 30 mM HEPES and 70 mM glycerol during the time span of a typical trapping experiment. The viability of MCF-7 cells under electric field conditions was also tested and revealed a significant increase in the dead/live ratio only at times larger than the typical trapping times (90 s). Under these conditions, the design for n-DEP trapping was used to demonstrate the proof-of-principle trapping design by successfully capturing a single MCF-7 cancer cell.

The novel device was utilized for distinctive iDEP trapping behavior of the two breast cancer cell types MCF-7 and MDA-MB-231 as well as B-lymphocytes. The device is capable of selecting single cells and selective trapping of single MCF-7 cells within a mixture containing B-lymphocytes or MDA-MB-231 was demonstrated. Experimental

observations were in excellent agreement with numerical simulations in which the trapping conditions for the various cell types were computed. It was further demonstrated that viable cells were trapped in the designed iDEP single cell trap and that the overall time and buffer conditions for iDEP-based single cell trapping relate well to conditions under which MCF-7 and MDA-MB-231 cells remain viable. The situation for PBMCs was different, indicating that the experimental conditions were less favorable for their viability. This might be expected for PBMCs, as they are not as resistant as tumor cells in stressful environments. Furthermore, the utility of this method would likely be used for tumor cell isolation and enrichment, not for PBMC isolation.

Experimental observations also indicate a distinctive change in iDEP properties for the two breast cancer cell types. It is postulated that these changes originate from differences in the invasive potential of each cell line related to distinctive phenotype differences. MDA-MB-231 cells express more vimentin [78] and have increased elastoviscosity [85]. The change in iDEP trapping behavior of the two cell types could originate from cytoplasmic as well as cell surface protein expression changes. Recently, changes in the cell glycocalyx originating from molecular brushes on the cell membrane have been reported for normal and cancerous human cervical epithelial cells [86] which could also have influences on  $\sigma_{mem}$  and thus the DEP response of different types of cancer cells.

The selectivity of weakly metastatic MCF-7 versus highly invasive MDA-MB-231 cells indicates that iDEP trapping could be employed as a diagnostic tool for cancer. Since the device has single cell selectivity, such an approach could be employed for the

detection of rare cancer cells. The parallelization of the presented single cell iDEP trap is straightforward and could be integrated within a microfluidic device to achieve high throughput in the future. To investigate the underlying biomolecular changes, such as variations in protein expression levels, one can also envisage coupling this iDEP device with a microfluidic platform for conducting MALDI MS analysis of proteins originating from single cells [61].

Development of the Generation-2 device is an improvement to the existing device with parallelized single cell traps. The central inlet connects the four channels which includes the trapping region at the center. The trapping regions were simulated and modified for optimized trapping conditions mainly for MCF-7 cancer cells. The first set of channels have four tear drop insulating posts as traps, whereas the second set of channels have two tear drop posts for trapping single cells. These devices are also adapted to be coupled with MADLI-MS detection in the side channels. They are also improved with a fifth channel for addressing the trapped cell with chemical lysing agent.

Future work would be directed towards testing of the Generation-2 device and coupling it with MALDI-MS. A more detailed viability study of the cancer cells is required for determining the optimized trapping condition of the cells. The approach for single cell trapping as presented in the Generation-2 device is a novel method for stimuli delivery to the cell trapping position as well as lysis and downstream transport for separation and detection. This multiplexed single cell trapping device would a first prototype of a total micro-analysis device designed for selective cancer cell analysis.

## REFERENCES

1. McClain MA, Culbertson CT, Jacobson SC, Allbritton NL, Sims CE, Ramsey JM (2003) Microfluidic devices for the high-throughput chemical analysis of cells. *Anal Chem* 75:5646-5655
2. Chao TC, Ros A (2008) Microfluidic single-cell analysis of intracellular compounds. *J R Soc Interface* 5 Suppl 2:S139-50
3. Roman GT, Chen Y, Viberg P, Culbertson AH, Culbertson CT (2007) Single-cell manipulation and analysis using microfluidic devices. *Anal Bioanal Chem* 387:9-12
4. Price AK, Culbertson CT (2007) Chemical Analysis of Single Mammalian Cells with Microfluidics. *Anal Chem* 79:2614-2621
5. Sims CE, Allbritton NL (2007) Analysis of single mammalian cells on-chip. *Lab Chip* 7:42-440
6. Desai JP, Pillarisetti A, Brooks AD (2007) Engineering approaches to biomanipulation. *Annu Rev Biomed Eng* 9:35-53
7. Grier DG (2003) A revolution in optical manipulation. *Nature* 424:810
8. Kim Y, Hong S, Lee SH, Lee K, Yun S, Kang Y, Paek KK, Ju BK, Kim B (2007) Novel platform for minimizing cell loss on separation process: Droplet-based magnetically activated cell separator. *Rev Sci Instrum* 78:074301
9. Han K, Frazier AB (2006) Paramagnetic capture mode magnetophoretic microseparator for high efficiency blood cell separations. *Lab Chip* 6:265-273
10. Gijs MAM (2004) Magnetic bead handling on-chip: new opportunities for analytical applications. *Microfluid Nanofluid* 1:22-40
11. Li Y, Dalton C, Crabtree HJ, Nilsson G, Kaler KVIS (2007) Continuous dielectrophoretic cell separation microfluidic device. *Lab Chip* 7:239-248
12. Rosenthal A, Taff BM, Voldman J (2006) Quantitative modeling of dielectrophoretic traps. *Lab Chip* 6:508-515
13. Gascoyne PRC, Vykoukal J (2002) Particle separation by dielectrophoresis. *Electrophoresis* 23:1973-1983

14. Choi S, Park J (2007) Continuous hydrophoretic separation and sizing of microparticles using slanted obstacles in a microchannel. *Lab Chip* 7:890-897
15. Neild A, Oberti S, Radziwill G, Dual J (2007) Simultaneous positioning of cells into two-dimensional arrays using ultrasound. *Biotechnol Bioeng* 97:1335-1339
16. Wiklund M, Gunther C, Lemor R, Jager M, Fuhr G, Hertz HM (2006) Ultrasonic standing wave manipulation technology integrated into a dielectrophoretic chip. *Lab Chip* 6:1537-1544
17. Kwon KW, Choi SS, Lee SH, Kim B, Lee SN, Park MC, Kim P, Hwang SY, Suh KY (2007) Label-free, microfluidic separation and enrichment of human breast cancer cells by adhesion difference. *Lab Chip* 7:1461-1468
18. Longo D, Hasty J (2006) Dynamics of single-cell gene expression. *Mol Syst Biol* 2:64
19. Yin H, Marshall D (2012) Microfluidics for single cell analysis. *Curr Opin Biotechnol* 23:110-119
20. Lindstrom S, Andersson-Svahn H (2010) Overview of single-cell analyses: microdevices and applications. *Lab Chip* 10:3363-3372
21. Burger R, Ducree J (2012) Handling and analysis of cells and bioparticles on centrifugal microfluidic platforms. *Expert Rev Mol Diagn* 12:407-21
22. Pethig R (2010) Dielectrophoresis: Status of the theory, technology, and applications. *Biomicrofluidics* 4:022811
23. Voldman J (2006) Electrical forces for microscale cell manipulation. *Annu Rev Biomed Eng* 8:425-441
24. Voldman J, Braff RA, Toner M, Gray ML, Schmidt MA (2001) Holding forces of single-particle dielectrophoretic traps. *Biophys J* 80:531-541
25. Schnelle T, Muller T, Gradl G, Shirley SG, Fuhr G (2000) Dielectrophoretic manipulation of suspended submicron particles. *Electrophoresis* 21:66-73
26. Magnus S J, Katja U, Thomas STM (2000) Contact-free single-cell cultivation by negative dielectrophoresis. *J.Appl.Phys*:175502
27. Thomas RS, Morgan H, Green NG (2009) Negative DEP traps for single cell immobilisation. *Lab Chip* 9:1534-1540

28. Thomas RS, Mitchell PD, Oreffo RO, Morgan H (2010) Trapping single human osteoblast-like cells from a heterogeneous population using a dielectrophoretic microfluidic device. *Biomicrofluidics* 4:10.1063
29. Gray DS, Tan JL, Voldman J, Chen CS (2004) Dielectrophoretic registration of living cells to a microelectrode array. *Biosens Bioelectron* 19:1765-1774
30. Sedgwick H, Caron F, Monaghan PB, Kolch W, Cooper JM (2008) Lab-on-a-chip technologies for proteomic analysis from isolated cells. *J R Soc Interface* 5 Suppl 2:S123
31. Jang LS, Huang PH, Lan KC (2009) Single-cell trapping utilizing negative dielectrophoretic quadrupole and microwell electrodes. *Biosens Bioelectron* 24:3637-3644
32. Cui HH, Lim KM (2009) Pillar array microtraps with negative dielectrophoresis. *Langmuir* 25:3336-3339
33. Bocchi M, Lombardini M, Faenza A, Rambelli L, Giulianelli L, Pecorari N, Guerrieri R (2009) Dielectrophoretic trapping in microwells for manipulation of single cells and small aggregates of particles. *Biosens Bioelectron* 24:1177-1183
34. Hunt TP, Westervelt RM (2006) Dielectrophoresis tweezers for single cell manipulation. *Biomed Microdevices* 8:227-230
35. Huang CT, Weng CH, Jen CP (2011) Three-dimensional cellular focusing utilizing a combination of insulator-based and metallic dielectrophoresis. *Biomicrofluidics* 5:44101
36. Hakoda M, Wakizaka Y, Hirota Y (2010) Separation of viable and nonviable animal cell using dielectrophoretic filter. *Biotechnol Prog* 26:1061-1067
37. Lapizco-Encinas B, Simmons BA, Cummings EB, Fintschenko Y (2004) Dielectrophoretic Concentration and Separation of Live and Dead Bacteria in an Array of Insulators. *Anal Chem* 76:1571-1579
38. Jen C, Chen T (2009) Selective trapping of live and dead mammalian cells using insulator-based dielectrophoresis within open-top microstructures. *Biomed Microdevices* 11:597-607
39. Racila E, Euhus D, Weiss AJ, Rao C, McConnell J, Terstappen LWMM, Uhr JW (1998) Detection and characterization of carcinoma cells in the blood. *Proc Natl Acad Sci* 95:4589
40. Nilsson J, Evander M, Hammarström B, Laurell T (2009) Review of cell and particle trapping in microfluidic systems. *Anal Chim Acta* 649:141-157

41. Mostert B, Sleijfer S, Foekens JA, Gratama JW (2009) Circulating tumor cells (CTCs): detection methods and their clinical relevance in breast cancer. *Cancer Treat Rev* 35:463-474
42. Yang J, Huang Y, Wang X, Wang XB, Becker FF, Gascoyne PR (1999) Dielectric properties of human leukocyte subpopulations determined by electrorotation as a cell separation criterion. *Biophys J* 76:3307-3314
43. Wang X, Yang J, Huang Y, Vykoukal J, Becker FF, Gascoyne PRC (2000) Cell Separation by Dielectrophoretic Field-flow-fractionation. *Anal Chem* 72:832-839
44. Wang X, Huang Y, Burt J, Markx G, Pethig R (1993) Selective dielectrophoretic confinement of bioparticles in potential energy wells. *J Phys D* 26:1278
45. Braschler T, Demierre N, Nascimento E, Silva T, Oliva AG, Renaud P (2008) Continuous separation of cells by balanced dielectrophoretic forces at multiple frequencies. *Lab Chip* 8:280-286
46. Valero A, Braschler T, Demierre N, Renaud P (2010) A miniaturized continuous dielectrophoretic cell sorter and its applications. *Biomicrofluidics* 4:10.1063
47. An J, Lee J, Lee SH, Park J, Kim B (2009) Separation of malignant human breast cancer epithelial cells from healthy epithelial cells using an advanced dielectrophoresis-activated cell sorter (DACS). *Anal Bioanal Chem* 394:801-809
48. Park J, Kim B, Choi SK, Hong S, Lee SH, Lee K (2005) An efficient cell separation system using 3D-asymmetric microelectrodes. *Lab Chip* 5:1264-1272
49. Cummings EB, Singh AK (2003) Dielectrophoresis in microchips containing arrays of insulating posts: theoretical and experimental results. *Anal Chem* 75:4724-4731
50. Baylon-Cardiel JL, Lapizco-Encinas BH, Reyes-Betanzo C, - Chavez-Santoscoy AV, Martinez-Chapa SO (2009) Prediction of trapping zones in an insulator-based dielectrophoretic device. - *Lab Chip* 28: 2896-2901
51. Lapizco-Encinas BH, Rito-Palomares M (2007) Dielectrophoresis for the manipulation of nanobioparticles. *Electrophoresis* 28:4521-4538
52. Ozuna-Chacon S, Lapizco-Encinas BH, Rito-Palomares M, Martinez-Chapa SO, Reyes-Betanzo C (2008) Performance characterization of an insulator-based dielectrophoretic microdevice. *Electrophoresis* 29:3115-3122

53. Lapizco-Encinas B, Simmons BA, Cummings EB, Fintschenko Y (2004) Insulator-based dielectrophoresis for the selective concentration and separation of live bacteria in water. *Electrophoresis* 25:1695-1704
54. Moncada-Hernandez H, Baylon-Cardiel JL, Pérez-González VH, Lapizco-Encinas BH (2011) Insulator-based dielectrophoresis of microorganisms: Theoretical and experimental results. *Electrophoresis* 32:2502-2511
55. Kang Y, Li D, Kalams S, Eid J (2008) DC-Dielectrophoretic separation of biological cells by size. *Biomed Microdevices* 10:243-2511
56. Jesus-Perez NM, Lapizco-Encinas BH (2011) Dielectrophoretic monitoring of microorganisms in environmental applications. *Electrophoresis* 17:2331-2357
57. Jones P, Staton S, Hayes M (2011) Blood cell capture in a sawtooth dielectrophoretic microchannel. *Anal Bioanal Chem* 401:2103-2111
58. Shafiee H, Sano MB, Henslee EA, Caldwell JL, Davalos RV (2010) Selective isolation of live/dead cells using contactless dielectrophoresis (cDEP). *Lab Chip* 10:438-445
59. Sano MB, Henslee EA, Schmelz E, Davalos RV (2011) Contactless dielectrophoretic spectroscopy: Examination of the dielectric properties of cells found in blood. *Electrophoresis* 32:3164-3171
60. Sano MB, Caldwell JL, Davalos RV (2011) Modeling and development of a low frequency contactless dielectrophoresis (cDEP) platform to sort cancer cells from dilute whole blood samples. *Biosens Bioelectron* 30:13-20
61. Yang M, Chao TC, Nelson R, Ros A (2012) Direct detection of peptides and proteins on a microfluidic platform with MALDI mass spectrometry. *Anal Bioanal Chem* 404(6-7): 1681-1689
62. Andrews AT, (1981), *Electrophoresis, Theory, Techniques and Biochemical and Clinical Applications*, Clarendon Press, Oxford
63. Schulz S, Sticher H (1994) Surface charge densities and electrophoretic mobilities of aqueous colloidal suspensions of latex spheres with different ionizable group. *Prog. Polym. Sci.* 97: 85-88
64. Swinney K, Bornhop DJ (2000) Detection in capillary electrophoresis. *Electrophoresis* 21:1239-1250

65. Miura K (2001) Imaging and detection technologies for image analysis in electrophoresis. *Electrophoresis* 22:801-813
66. Viefhues M, Manchanda S, Chao T, Anselmetti D, Regtmeier J, Ros A (2011) Physisorbed surface coatings for poly(dimethylsiloxane) and quartz microfluidic devices. *Anal Bioanal Chem* 401:2113-2122
67. Pohl HA (1978) Dielectrophoresis the behavior of neutral matter in nonuniform electric fields, Cambridge University Press, Cambridge
68. Jones T.B (1995) *Electromechanics of Particles*, Cambridge University Press, New York
69. Kwon J, Maeng J, Chun M, Song S (2008) Improvement of microchannel geometry subject to electrokinesis and dielectrophoresis using numerical simulations. *Microfluidic Nanofluid* 5:23-31
70. Cui L, Holmes D, Morgan H (2001) The dielectrophoretic levitation and separation of latex beads in microchips. *Electrophoresis* 22:3893-3901
71. Arnold WM (1987) Surface conductance and other properties of latex particles measured by electrorotation. *J. Phys. Chem, A* 91:5093-5098
72. Ros A, Eichhorn R, Regtmeier J, Duong TT, Reimann P, Anselmetti D (2005) Brownian motion: absolute negative particle mobility. *Nature* 436:928
73. Regtmeier J, Grauwin S, Eichhorn R, Reimann P, Anselmetti D, Ros A (2007) Acceleration of absolute negative mobility. *J Sep Sci* 30:1461-1467
74. Grossman PD, Colburn JC (1992) *Capillary Electrophoresis-Theory and Practice*. Academic Press; San Diego
75. Martinez-Lopez JI, Moncada-Hernandez H, Baylon-Cardiel JL, Martinez-Chapa SO, Rito-Palomares M, Lapizco-Encinas BH (2009) Characterization of electrokinetic mobility of microparticles in order to improve dielectrophoretic concentration. *Anal Bioanal Chem* 394:293-302
76. Sommers CL, Byers SW, Thompson EW, Torri JA, Gelmann EP (1994) Differentiation state and invasiveness of human breast cancer cell lines. *Breast Cancer Res Treat* 31:325-335
77. Thompson EW, Paik S, Brünner N, Sommers CL, Zugmaier G, Clarke R, Shima TB, Torri J, Donahue S, Lippman ME. (1992) Association of increased basement

membrane invasiveness with absence of estrogen receptor and expression of vimentin in human breast cancer cell lines. *J Cell Physiol* 150:534-544

78. Lacroix M, Leclercq G (2004) Relevance of breast cancer cell lines as models for breast tumours: an update. *Breast Cancer Res Treat* 83:249-289

79. Zeisberg MM, Neilson EG (2009) Biomarkers for epithelial-mesenchymal transitions. *The Journal of clinical investigation* 119:1429-1437

80. Hu QQ (2009) Model study of electroporation effects on the dielectrophoretic response of spheroidal cells. *J Appl Phys* 106:024701

81. Bordi F, Cametti C, Rosi A, Calcabrini A (1993) Frequency domain electrical conductivity measurements of the passive electrical properties of human lymphocytes. *Nucleus* 1153:77-88

82. Chuang CH, Huang YW, Wu YT (2011) System-level biochip for impedance sensing and programmable manipulation of bladder cancer cells. *Sensors* 11:11021

83. Timonen T, Ortaldo JR, Herberman RB (1981) Characteristics of human large granular lymphocytes and relationship to natural killer and K cells. *J Exp Med* 153:569-582

84. Henslee EA, Sano MB, Rojas AD, Schmelz EM, Davalos RV (2011) Selective concentration of human cancer cells using contactless dielectrophoresis. *Electrophoresis* 32:2523-2529

85. Lee MH, Wu PH, Staunton JR, Ros R, Longmore GD, Wirtz D (2012) Mismatch in mechanical and adhesive properties induces pulsating cancer cell migration in epithelial monolayer. *Biophys J* 102:2731-2741

86. Iyer S, Gaikwad RM, Subba-Rao V, Woodworth CD, Sokolov I (2009) Atomic force microscopy detects differences in the surface brush of normal and cancerous cells. *Nat Nanotechnol* 4:389-393

## APPENDIX A

## SIMULATIONS WITH COMSOL

The COMSOL simulation software was used for mapping the trapping regions in the microfluidic devices using Eq. 21. Several modules are available for creating the desired simulation with the appropriate physics.

### 1. Geometry

The geometry is created in AutoCAD and exported to COMSOL in the “.dxf” format. The software is also equipped with a drawing module which can be helpful to further improve the device geometry. The unit of the drawing module is set to  $\mu\text{m}$  dimensions. The geometries for the insulating posts are created in AutoCAD. The inner and outer radius of the tear-drop is created using the *Arc* module of AutoCAD. The geometric lines drawn to a circle are joined together with the arc of a desired radius. This radius defines the tip of the post. The lines of the geometry are all connected using the Auto CAD module *Polylines*. This module joins the geometry together in one complete unit. This complete unit is easily exported in COMSOL as a solid geometry.

### 2. Model

The 2-dimensional model is chosen for the geometry space. A 3-dimensional model can also be applied but is not necessary for the simulations used in this work. There are several physics modules that are chosen to be applied to solving the desired conditions.

- a. *Electric currents*: The geometry boundaries are set as insulators by default. This module chooses the geometry boundaries required to be conductive. The

required potential can also be set at those boundary walls. The wall boundaries which are set as insulating follow the boundary condition as given:

$$\mathbf{n} \cdot \mathbf{J} = 0 \quad (\text{A1})$$

where,  $\mathbf{J}$  is current density and  $\mathbf{n}$  is unit vector. This boundary condition specifies that no current flows across the boundary. Electrical potential specifies the electrical potential as  $V = V_0$  at the boundary condition, where  $V_0$  is the user defined potential (SI unit: V).

- b. *Creeping flow*: This module defines the type of fluid flow in the device. The Reynolds number for the fluid flow in this system is below 1, hence this module is best suited for the system.

The sub-module, *open boundary*, defines the pressure at the inlet and outlet. The formula used to define the normal stress at the boundary is given as:

$$(-p + \eta(\nabla \mathbf{v} + (\nabla \mathbf{v})^T)) = \mathbf{f} \quad (\text{A2})$$

where,  $p$  is the pressure,  $\eta$  is user defined fluid viscosity,  $\mathbf{v}$  is fluid and  $\mathbf{f}$  is force.  $\nabla$  is *del operator* and  $T$  is *Lagrangian operator*. For open boundaries, the pressure  $p$  is zero and the initial fluid velocity is zero.

The sub-module, *fluid properties*, defines the dynamic viscosity ( $1.0009 \times 10^{-3}$  Pa·sec) and density ( $1 \times 10^{-3}$  kg·m<sup>3</sup>).

The sub-module, *wall*, defines the flow conditions at the wall taking into consideration a no slip condition at the immediate wall surface and

electroosmotic flow (EOF) throughout the channel. The equation for the electroosmotic velocity is given as:

$$\mathbf{v}_{eof} = \mu_{eof} \mathbf{E} \quad (\text{A3})$$

where  $\mu_{eof}$  is the user defined mobility and  $\mathbf{E}$  is applied electric field and  $\mathbf{v}_{eof}$  is the electroosmotic velocity. This velocity is taken as the fluid velocity for the entire simulation. The EOF is defined in the main text in Chapter 2.

### 3. Materials

The materials module is used to define the variables used in the simulation, mainly the fluidic properties and user defined values like EOF and DEP mobility.

The main variables defined in the system are:

$\mu_{eof}$ : electroosmotic mobility of the fluid,  $\boldsymbol{\eta}$ : fluid viscosity,  $\mu_{dep}$ : dielectrophoretic mobility of the particle and  $r$ : particle radius.

### 4. Mesh

The *mesh* is defined as free triangles. This mesh divides the geometry space into many triangles and solves for the required value. The defined free triangle is chosen as it gives the least error in the solution. The mesh is set as a *Fine mesh* for the complete geometry in which a homogeneous distribution of areas are established so that the calculated solution is unbiased and uniform (*i.e.* certain areas do not give rise to a non-uniform distribution of points or areas to be solved). The *Very Fine mesh* is generally not used as the solutions become non-solvable near the tips of the posts.

## 5. Solution

The stationary solution module is chosen as the condition used for the simulation is DC. This module accepts the defined physics and solves for the required parameters.

## 6. Results

The *results* have sub-modules which are used to define the desired results. The 2D sub-module is chosen for this purpose and the area plot defines the trapping region in the defined geometry according to Eq. 21. This equation translates to:

$$\left( \frac{d(ec.E_x^2 + ec.E_y^2, x) * ec.E_x + (d(ec.E_x^2 + ec.E_y^2, y) * ec.E_y)}{(ec.E_x^2 + ec.E_y^2)} \right) * r$$

where,  $r = \frac{\mu_{DEP}}{\mu_{EOF}}$  and  $ec.E_x$ ,  $ec.E_y$  is electric field for X and Y-coordinate respectively. The *surface* plot shows the region where the trapping condition is achieved.